Design and Testing of Off-The-Shelf Electronic Components for an Acoustic Emission Structural Health Monitoring System Using Piezoelectric Sensors

Yiu Kui Law

Thesis submitted to the Faculty of the
Virginia Polytechnic Institute and State University
in partial fulfillment of the requirements of the degree of

Master of Science
in
Mechanical Engineering

Dr. Alfred L. Wicks, Chair
Dr. Harry H. Robertshaw, Committee
Dr. Martin E. Johnson, Committee

August, 2005
Blacksburg, Virginia

Keywords: acoustic emission, operational amplifier, charge amplifier, high pass filter, low pass filter, line driver

Design and Testing of Off-The-Shelf Electronic Components for an Acoustic Emission Structural Health Monitoring System Using Piezoelectric Sensors

Yiu Kui Law

Abstract

The safety concern of aging aircraft is a rising issue in terms of both safety and cost. An aircraft structure failure during flight is unacceptable. A method needs to be developed and standardized to test the integrity of both commercial and military aircrafts. The current method to test the structure of an aircraft requires the aircraft to be taken out of service for inspection; this is costly due to the inspection required to be performed and the lost use from downtime.

A novice idea of an on-site structural health monitoring (SHM) system has been proposed to test the integrity of aircraft structure. An on-site system is a system that can be used to perform inspection on an aircraft simultaneously while the aircraft is in use. This SHM system uses the principles of active lamb wave and passive acoustic emission through the use of piezoelectric sensors as the sensing elements. Piezoelectric sensors can be used both as an input device and as a sensing element.

This research focuses on the development of the major data acquisition electronic components of the system. These components are charge amplifier, high pass filter, low pass filter and line driver. A charge amplifier converts a high impedance signal to a low impedance signal. A high pass filter attenuates the low frequency content of a signal, while a low pass filter attenuates the high frequency content of a signal. A line driver converts a low current signal to a high current signal. All of these components need to operate up to a frequency of 2 MHz. Off-the-shelf electronics will be used for prototyping as custom components will not be feasible at this point of the research.

Acknowledgements

While I have many people to thank, I would like to thank Dr. Wicks for giving me the opportunity to work on this project. As incompetent as I was in the field of electronics, Dr. Wicks has given the patience and guidance for me to explore. While this project has given me a great deal of frustration, it was no doubt a rewarding one. It also made me realized how little I know and the learning curve does not end here.

I would also like to thank Dr. Robertshaw for providing me with funding as a Graduate Teaching Assistant for the year of 2003-2004. Without this funding, I probably would not have been able to continue graduate school. Being a TA for ME 4016 also taught me a great deal in terms of teaching other fellow students, which required a tremendous amount of patience. I also like to thank Dr. Robertshaw and Dr. Johnson for serving on my committee. Dr. Johnson gave me the opportunity to do undergraduate research, which motivated me to continue graduate studies.

Special thanks go to my parents who have sacrificed so much to move from Hong Kong to the United States so my brother and I could have a better life. My dad gave up his own business in Hong Kong to work in the US making a little more than minimum wage. What they have sacrificed is indescribable. For that, I am forever indebted. I also need to thank my brother who has always set the bar so high that it will be a shame if I don't follow his footstep.

To all the wonderful friends I have made here at Virginia Tech in the last seven years, thank you. Without you, I would not have been able to survive. A special thank goes to my best friend, Travis Dillon, who has always looked out for me ever since we became roommates in our freshmen year. We started college together, and we finished college together. I am truly blessed to have a friend like him.

A few people cannot be forgotten. Randy Smith has helped and taught me soldering skill, which I had known nothing before. Pen Poe and Jamie Archual helped me a great deal whenever I had computer problems. Cathy Hill, Jan Riess and Lynne Ellis have provided help for all the administrative work throughout my graduate and undergraduate careers. I also need to thank John Bird and Kalyanramu Vemishetty for their continue support.

Last but not least, I would like to thank my very special friend, Theresa Cho, who has been nothing but supportive throughout my struggle in the last year. She was always patient and listened when I complained to her. All the support she gave me was what drove me to keep going and never quit. Knowing her has been the best thing that ever happened to me. Thank you, Theresa.

Table of Contents

List of Figures

List of Tables

1 Introduction

This research is sponsored by the Air Force and is a collaborative effort among three groups: Triad Semiconductor Inc., The University of South Carolina and The North Carolina A&T State University. The goal is to develop a prototype structural health monitoring (SHM) system using off-the-shelf electronics to be tested on real aircraft panels. Triad Semiconductor Inc. provides the electronic design and signal processing development. The University of South Carolina provides the active lamb wave technology, while The North Carolina A&T State University provides the passive acoustic emission expertise.

1.1 Motivation of Research

The maintenance cost for aging aircraft is about 24% of a commercial airline's operating cost [4]. With more aircrafts operating beyond their design operating cycle, the structural integrity of aging aircrafts has raised increased concern. The current method to test aircraft structural integrity requires the aircraft to be taken out of service for inspections; this drastically increases both the cost for inspection and the cost for lost use [4]. An on-site material-integrated structural health monitoring (SHM) system using piezoelectric sensors has been proposed. An on-site system is a system that continuously checks the aircraft's structural integrity while the aircraft is in use. One common type of piezoelectric materials is the Lead Zirconate Titanate (PZT). PZT sensors can perform both the sensing ability as a transducer and the input ability as an actuator.

In general, there are two ways to use piezoelectric sensors in this structural health monitoring system: active lamb wave and passive acoustic emission [17]. In an active lamb wave system, a sensor applies an input lamb wave (or other types of waves) to the structure while the other sensors detect the reflected signal [10]. In a passive acoustic emission system, the sensors sense the release of strain energy from the structure as a result of propagation of crack [2, 14]. Using information such as the voltage signal from various sensors and the geometry of the structure, a defect in the material can be approximated.

1.2 Objective of Research

The primary objective of this research is to design and test the necessary electronic components in order to develop a prototype SHM system. Since both lamb wave and acoustic emission operate in a frequency range of MHz, these electronics need to perform well in the high frequency range. This system will incorporate both the active lamb wave and passive acoustic emission technologies into one integrated multi-sensor system. Since the concept of integrating both techniques into one system is still quite novel, off-the-shelf components will mainly be used for design and testing for the electronics. Also Labview 7.1 Express and Labview data acquisition card (DAQ) will be used for interfacing the circuit boards to a PC after the design of these electronics are finalized.

The development and prototyping phase of this research is to successfully build a system that will be used to test on a simple aluminum plate with eleven piezoelectric sensors bonded to the plate. A signal generator will be used to generate a known frequency sine wave into one of the sensors on the aluminum plate, and the signal will be sensed from other sensors on the plate into an oscilloscope.

Instead of the lamb wave and acoustic emission testing, the majority of the work in this thesis focused on the understanding of the structural health monitoring technology; the testing of numerous operational amplifiers; and the design and analysis of various circuits. Among these circuits tested were charge amplifier, high pass filter, low pass filter and line driver. When the prototype circuit board is successfully built and tested, it will be sent to both The University of South Carolina and The North Carolina A&T State University for testing. USC has the expertise in active lamb wave while NC A&T has the expertise in passive acoustic emission. These two universities will use this prototype system to perform various testing on both techniques. The Air Force will also use this system to test on real aircraft panels. The ultimate goal is to incorporate both technologies into one integrated sensor system.

2 Background Information and Literature Review

This chapter introduces the basic principle of piezoelectric material, its properties and its mathematical formula [16]. Because both active lamb wave and passive acoustic emission technology are based on the principle of wave propagation, a brief introduction of the different types of waves and their mathematical formula will be presented [7, 8]. The two different structural health monitoring techniques: active lamb wave and passive acoustic emission, will be introduced [1, 19]. The different electronic components required to successfully design a prototype structural health monitoring (SHM) system will also be discussed [5].

2.1 Introduction to Piezoelectric Sensors

Discovered in 1880 by brothers Pierre and Jacques Curie [16], piezoelectricity describes the phenomenon of a certain ferroelectric material which generates an electric charge when it is subjected to a mechanical stress; and conversely, generates a mechanical strain when it is subjected to an applied electric field. Since the first discovery of piezoelectricity is that an electric charge is produced when a mechanical stress is applied to a material, this is called the direct piezoelectric effect. The discovery that a mechanical strain is produced when an applied electric field is applied to a material is thus called converse piezoelectric effect. To summarize,

1) direct piezoelectric effect – applied mechanical stress produces electric charge
2) converse piezoelectric effect – applied electric field produces mechanical strain

Due to this coupling relationship between the mechanical property and the electrical property, piezoelectric materials can perform both sensing and actuating functions. The sensing function works according to the direct piezoelectric effect, while the actuating function works according to the converse piezoelectric effect.

A piezoelectric material itself does not exhibit this mechanical and electrical relationship, it has to go through a poling process for it to exhibit this relationship. A piezoelectric sensor is a thin piece of piezoelectric material that is bonded to a structure, it is wired to a signal processing system that allows the sending and receiving of signals to the structure.

2.1.1 Piezoelectricity Formulation

For a piezoelectric material, an electric charge can be produced by applying a mechanical stress to the material, or a mechanical strain can be produced by applying an electric field to the material, there is a coupling relationship between the mechanical property and the electrical property [8, 16]. The mechanical relationship between stress and strain is

$$T = cS \tag{2.1}$$

where T is the stress [N/m^2], S is the strain [m/m] and c is the Young's Modulus [N/m^2]. Equation 2.1 can also be written in

$$S = sT \tag{2.2}$$

where s is called the elastic compliance [m^2/N]. The electrical relationship between electric field and electric displacement is

$$D = \varepsilon E \tag{2.3}$$

where E is the electric field [V/m], D is the electric displacement with unit of Coulombs per unit area [C/m^2] and ε is the dielectric permittivity with unit of Farads per meter [F/m]. The electric displacement can be thought of as the amount of charge that moves per unit area between two charged plates when subjected to a voltage potential.

Putting equations 2.2 and 2.3 in matrix form results in a two by two matrix algebraic equation

$$\begin{Bmatrix} S \\ D \end{Bmatrix} = \begin{bmatrix} s & 0 \\ 0 & \varepsilon \end{bmatrix} \begin{Bmatrix} T \\ E \end{Bmatrix} \tag{2.4}$$

where the top equation is the mechanical relationship and the bottom equation is the electrical relationship. However, for a piezoelectric material, there is a coupling relationship between the mechanical property and the electrical property. Therefore, the off-diagonal terms should be non-zero. These two off-diagonal terms are called the piezoelectric strain coefficients, d, and is the material property of a piezoelectric material. In order to define the piezoelectric equation completely, two boundary conditions exist. These two boundary conditions are zero electric field ($E = 0$) and zero mechanical stress ($T = 0$) respectively. The final piezoelectric equation is

$$\begin{Bmatrix} S \\ D \end{Bmatrix} = \begin{bmatrix} s^E & d \\ d & \varepsilon^T \end{bmatrix} \begin{Bmatrix} T \\ E \end{Bmatrix} \tag{2.5}$$

where S is the mechanical strain [m/m], D is the electric displacement [C/m^2], T is the mechanical stress [N/m^2], E is the electric field [V/m], s^E is the elastic compliance [m^2/N] measured under zero electric field, ε^T is the dielectric permittivity [F/m] measured under zero mechanical stress, and d is the piezoelectric strain coefficient.

In general, a piezoelectric material is modeled as three dimensional. Thus the mechanical equation in equation 2.5 would expand into six algebraic equations (S_1 to S_6) and the electrical equation would expand into three algebraic equations (D_1 to D_3). It is this mechanical and electrical coupling characteristic of a piezoelectric material that makes it one of the most popular materials for transducer and actuator purposes.

2.2 Introduction to Wave Propagation

Both active lamb wave and passive acoustic emission technologies used in this structural health monitoring system rely on the use of input and output waves on the structure for actuating and sensing. Thus a brief introduction to the different types of waves and their equations are presented. There are mainly five types of waves and each of them exhibits a different phenomenon and has its own sets of equations [7, 8]. Table 2-1 summarizes the five types of waves. The following sections present the wave equations for the different types of waves shown in Table 2-1. The wave propagation is assumed to be in the horizontal *x* direction. Section 2.2.5 presents a pictorial representation of each wave [3].

Table 2-1. Summary of elastic waves in a structure [8].

Wave Type	**Particle Motion**
Pressure (longitudinal, compressional, P-wave, axial)	Parallel to the direction of wave propagation
Shear (transverse, distortional, S-wave)	Perpendicular to the direction of wave propagation
Flexural (bending)	Elliptical, plane sections remain plane
Rayleigh (surface acoustic waves, or SAW)	Elliptical, amplitude decays quickly with depth
Lamb (guided, plate)	Elliptical, free surface conditions satisfied at the upper and lower plate surfaces

2.2.1 Pressure Wave

Pressure wave, also called longitudinal wave, compressional wave, axial wave or P-wave, has particle displacement parallel to the direction of propagation. Assuming wave propagation in a 1-D beam, the wave equation of a pressure wave is

$$u_x(x,t) = u_0 \times e^{i(k_P x - wt)} \tag{2.6}$$

in which u_x is the particle displacement in the direction of propagation, u_0 is the amplitude, k_P is the wave number, w is the angular frequency in [rad/s] and t is time in [s]. The wave number, k_P, can be written in terms of the wave speed, c_P and angular frequency, w as

$$k_P = \frac{w}{c_P} = \frac{2\pi}{\lambda} \tag{2.7}$$

where λ is the wavelength. For one dimensional wave propagation, the wave speed is

$$c_P = \sqrt{\frac{E}{\rho}} \tag{2.8}$$

in which E is the Young's Modulus and ρ is the density of the material in which the wave travels in. For three dimensional solid, the wave speed is

$$c_P = \sqrt{\frac{\lambda + 2\mu}{\rho}} \tag{2.9}$$

where λ and μ are called the Lamé constants and are defined as

$$\lambda = \frac{\nu E}{(1-2\nu)(1+\nu)} \qquad and \qquad \mu = \frac{E}{2(1+\nu)} \tag{2.10}$$

in which E is the Young's Modulus and ν is the Poisson's Ratio.

2.2.2 Shear Wave

Shear wave, also called transverse wave, distortional wave or S-wave, has the particle displacement perpendicular to the direction of propagation. Assuming wave propagation in a 2-D plane, the wave equation of a shear wave is

$$u_y(x,t) = u_0 \cdot e^{i(k_S x - wt)} \tag{2.11}$$

where u_y is the particle displacement perpendicular to the direction of propagation, u_0 is the amplitude, k is the wave number, w is the angular frequency in [rad/s] and t is time in [s]. The wave number, k_S, can be written in terms of the angular frequency, w, and wave speed, c_S,

$$k_S = \frac{w}{c_S} \tag{2.12}$$

The wave speed c_S is

$$c_S = \sqrt{\frac{\mu}{\rho}} \tag{2.13}$$

where ρ is the density of the material in which the wave travels in and μ is one of two Lamé constants defined in equation 2.10.

2.2.3 Flexural Wave

Flexural wave, also called bending wave, results from the bending action of a material. The simplest bending wave comes from the Bernoulli-Euler Beam Theory, which assumes that the effects of shear deformation and rotary inertial are negligible. The wave equation of a flexure wave is derived from the following 4th order partial differential equation [7], which requires the separation of variable method to solve. Assuming a 2-D plane, the governing equation is

$$\frac{\partial^4 u_y}{\partial x^4} + \frac{1}{a^2}\frac{\partial^2 u_y}{\partial t^2} = 0 \qquad and \qquad a^2 = \frac{EI}{\rho A} \tag{2.14}$$

In terms of the material in which the wave travels in, E is the Young's Modulus, I is the moment of inertia, ρ is the density and A is the cross sectional area. After solving this equation, the wave equation is

$$u_y(x, y, t) = u_0 \cdot e^{i(k_F x - wt)} \tag{2.15}$$

where u_y is the vertical particle displacement of the wave propagation, u_0 is the amplitude, k_F is the wave number, w is the angular frequency in [rad/s] and t is time [s]. For a beam, the moment of inertia is

$$I = \frac{bh^3}{12} \tag{2.16}$$

where b is the width of the cross section and h is the height of the cross section. The wave number k_F is defined as

$$k_F = \sqrt{\frac{w}{a}} \tag{2.17}$$

The wave speed, c_F, can also be written in terms of the angular frequency, w

$$c_F = ak_F = \sqrt{aw} \tag{2.18}$$

2.2.4 Rayleigh Wave

Rayleigh wave, also called surface acoustic waves (SAW), has its propagation on the surface of the material with the motion amplitude decreasing with depth. Rayleigh wave has two components in the wave equation; a horizontal component (u_x) and a vertical component (u_y). Assuming a cross section perpendicular to the body surface of a 2-D plane, these two wave equations are defined as

$$\begin{aligned} u_x(x,y,t) &= u_0 k_R \left(e^{-qy} - \frac{2qs}{k_R^{\ 2} + s^2} e^{-sy} \right) e^{i(k_R x - wt)} \\ u_y(x,y,t) &= i u_0 q \left(e^{-qy} - \frac{2k_R^{\ 2}}{k_R^{\ 2} + s^2} e^{-sy} \right) e^{i(k_R x - wt)} \end{aligned} \tag{2.19}$$

where

$$q = \sqrt{k_R^{\ 2} - k_P^{\ 2}} \qquad and \qquad s = \sqrt{k_R^{\ 2} - k_S^{\ 2}} \tag{2.20}$$

Here u_0 is the amplitude, k_R is the Rayleigh wave number, k_P is the pressure wave number defined in equation 2.7, k_S is the shear wave number defined in equation 2.12, w is the angular frequency in [rad/s] and t is time [s]. The Rayleigh wave number, k_R, is also defined as

$$k_R = \frac{w}{c_R} \tag{2.21}$$

where c_R is the Rayleigh wave speed and can be approximated from the following

$$c_R = c_S \left(\frac{0.87 + 1.12\nu}{1 + \nu} \right) \tag{2.22}$$

where c_S is the shear wave speed defined in equation 2.13 and ν is the Poisson's Ratio of the material in which the wave travels in.

2.2.5 Lamb Wave

Lamb wave, also called guided plate wave, is a wave guided between two parallel surfaces. The particle displacement of Lamb wave is both perpendicular to the surface of the plate and parallel to the direction of propagation. There are two basic propagation types of Lamb wave: symmetric and anti-symmetric [7, 8, 12]. For each type of Lamb wave, there are also a number of modes associated with each type corresponding to the solutions of the wave equation. The symmetric modes are denoted as S_0, S_1, S_2… while the anti-symmetric modes are denoted as A_0, A_1, A_2… For the symmetric modes, the displacement and stress are symmetric. The boundary conditions are

$$u_x(x,d) = u_x(x,-d) \qquad and \qquad \tau_{yx}(x,d) = -\tau_{yx}(x,-d)$$
$$u_y(x,d) = -u_y(x,-d) \qquad and \qquad \tau_{yy}(x,d) = \tau_{yy}(x,-d)$$

For the anti-symmetric modes, the displacement and stress are anti-symmetric. The boundary conditions are

$$u_x(x,d) = -u_x(x,-d) \qquad and \qquad \tau_{yx}(x,d) = \tau_{yx}(x,-d)$$
$$u_y(x,d) = u_y(x,-d) \qquad and \qquad \tau_{yy}(x,d) = -\tau_{yy}(x,-d)$$

Figure 2-1 shows the difference between the boundary conditions for both the symmetric and anti-symmetric modes.

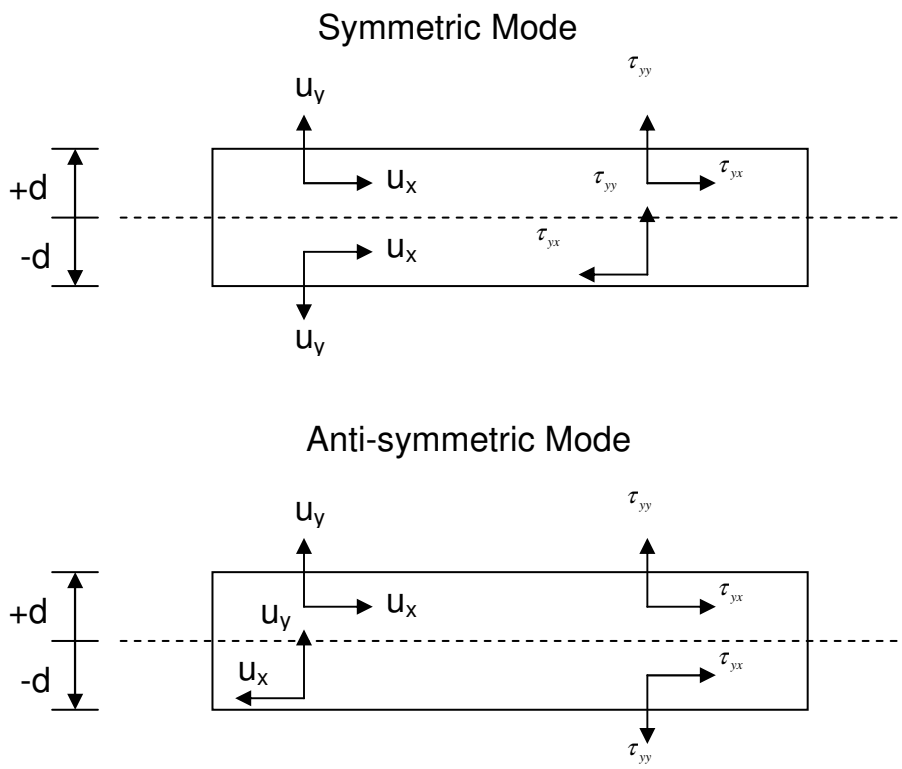

Figure 2-1. The boundary conditions for both symmetric and anti-symmetric Lamb modes [8].

At low frequencies, the symmetric modes behave similar to the axial wave, while the anti-symmetric modes behave similar to the flexural wave. The Lamb wave speed also depends on the product of frequency and plate thickness.

The Lamb wave equations are rather complicated and the derivation will not be presented here. The derivation can be found at [8]. Therefore, only the wave equations will be presented. The Lamb wave equation is a function of both frequency and the half thickness of the material. For the symmetric Lamb modes, assuming the wave propagation is guided between two parallel free surfaces, the wave equation is

$$\frac{\tan(pd)}{\tan(qd)} + \frac{4\xi^2 pq}{(\xi^2 - q^2)^2} = 0 \tag{2.23}$$

where the followings are defined

$$p = \sqrt{\frac{w^2}{c_P{}^2} - \xi^2} \qquad and \qquad q = \sqrt{\frac{w^2}{c_S{}^2} - \xi^2} \tag{2.24}$$

in which c_P and c_S are the pressure wave speed and shear wave speed defined in equations 2.9 and 2.13 respectively. Also, d is the half thickness of the material in which the wave travels in, and ξ are the eigenvalues, $\xi_0^S, \xi_1^S, \xi_2^S, ...$ to be solved for the different modes. Equation 2.23 requires numerical technique to solve and is a function of the product of the frequency, w, and half thickness, d. Numerical solution yields the following particle displacement equations

$$\begin{aligned} u_x &= -2\xi^2 q \cos(qd)\cos(py) + q(\xi^2 - q^2)\cos(pd)\cos(qy) \\ u_y &= -2i\xi\, pq \cos(qd)\sin(py) - i\xi(\xi^2 - q^2)\cos(pd)\sin(qy) \end{aligned} \tag{2.25}$$

The anti-symmetric Lamb wave equation takes a similar form as the symmetric Lamb wave equation in equation 2.23. Assuming the wave propagation is guided between two parallel free surfaces, the wave equation for the anti-symmetric Lamb mode is

$$\frac{\tan(pd)}{\tan(qd)} + \frac{(\xi^2 - q^2)^2}{4\xi^2 pq} = 0 \tag{2.26}$$

where p and q are defined in equation 2.24. The parameter d is the half thickness of the material as shown in Figure 2-1, and ξ are the eigenvalues, $\xi_0^A, \xi_1^A, \xi_2^A, ...$ to be solved for the different modes. Equation 2.26 requires numerical technique to solve and is a function of the product of the frequency, w, and half thickness, d. Numerical solution yields the following particle displacement equations

$$
\begin{aligned}
u_x &= -2\xi^2 q \sin(qd)\sin(py) + q(\xi^2 - q^2)\sin(pd)\sin(qy) \\
u_y &= 2i\xi\, pq \sin(qd)\cos(py) + i\xi(\xi^2 - q^2)\sin(pd)\cos(qy)
\end{aligned}
\tag{2.27}
$$

Figure 2-2 shows the wave speed for different waves including the symmetric and anti-symmetric Lamb waves in a typical aluminum test material. It shows that at low frequencies, the symmetric Lamb wave, S_0, behaves as the axial pressure wave, and the anti-symmetric Lamb wave, A_0, behaves as the flexural wave. Also, at high frequencies, both the symmetric and anti-symmetric Lamb waves behave like Rayleigh wave.

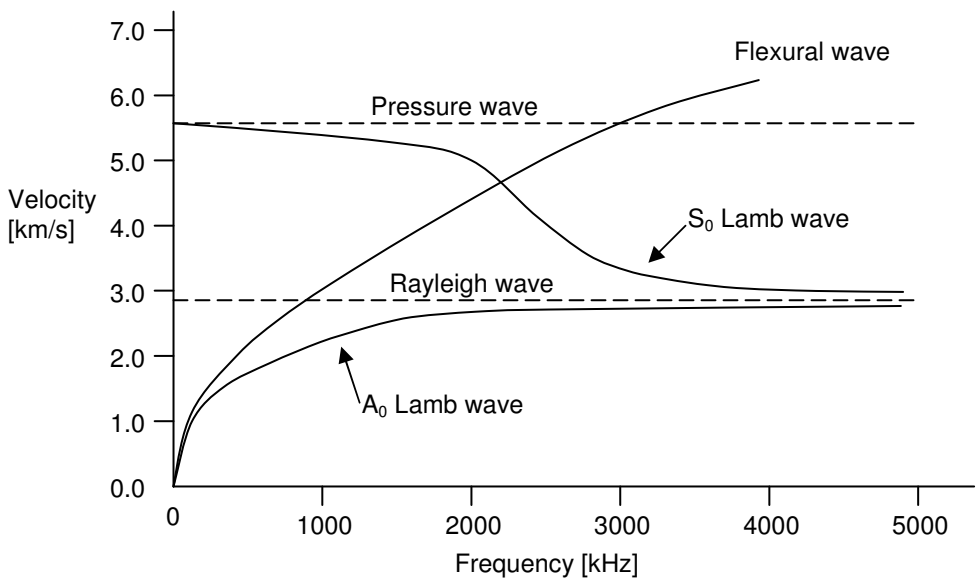

Figure 2-2. Calculation of frequency dependence of wave speed in 1-mm thick aluminum plate. Comparison of different waves shows that at low frequency, S_0 Lamb wave resembles axial pressure wave and A_0 Lamb wave resembles flexural wave [8].

2.2.6 Pictorial Representation of Different Waves

This section presents the pictorial representation of each wave [3, 8]. The wave propagation is in the horizontal direction for all the figures presented.

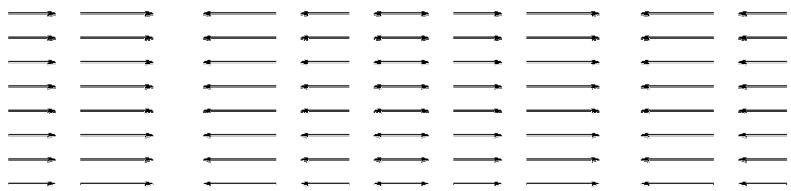

Figure 2-3. Pressure wave shows that the particle motion is parallel to the wave propagation. This is seen as the top view.

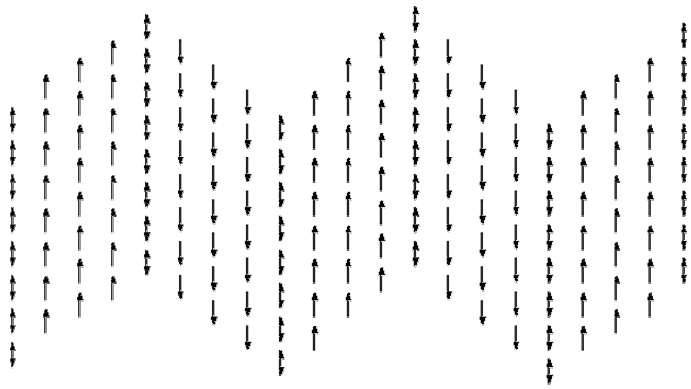

Figure 2-4. Shear wave shows that the particle motion is perpendicular to the direction of wave propagation. This is seen as the top view.

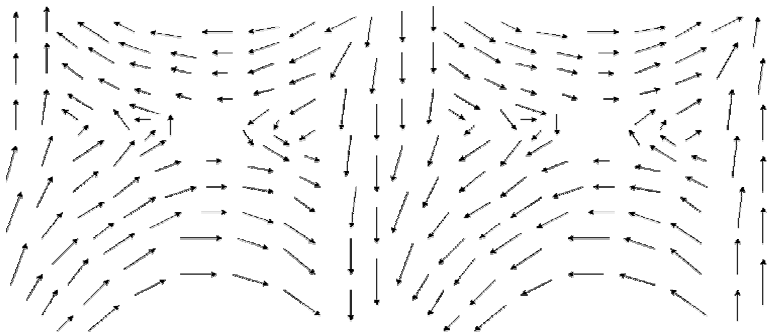

Figure 2-5. Flexural wave shows that the particle motion is planar and elliptical relative to the wave propagation. This is seen as the top view.

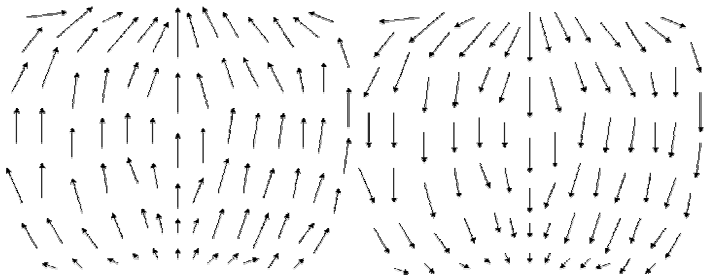

Figure 2-6. Rayleigh wave shows that the particle motion is elliptical relative to the wave propagation and the amplitude decreases with depth (shorter arrows at the bottom). This is seen as the side view.

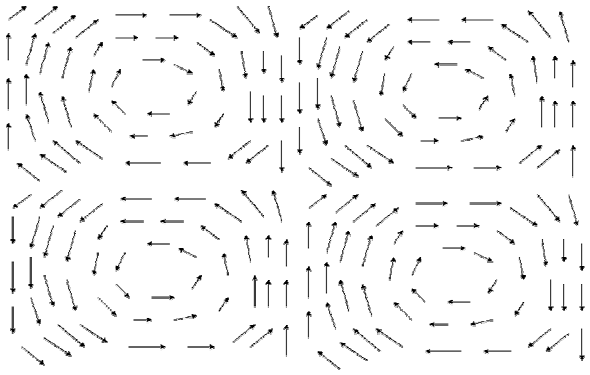

Figure 2-7. Symmetric Lamb wave shows that the particle motion is elliptical relative to the wave propagation and is bounded between the upper and lower surfaces. This is seen as the side view.

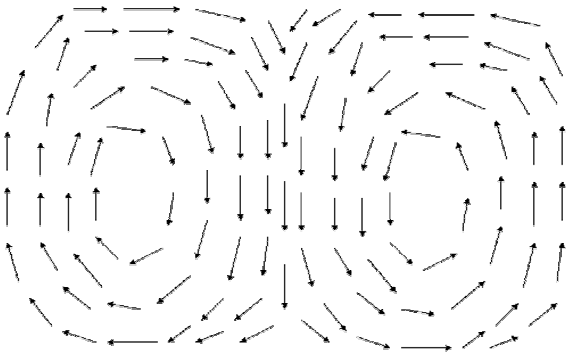

Figure 2-8. Anti-Symmetric Lamb waves shows that the particle motion is elliptical relative to the wave propagation and is bounded between the upper and lower surfaces. This is seen as the side view.

2.3 Introduction to Active Lamb Wave and Passive Acoustic Emission

The two different types of structural health monitoring techniques to detect defects in a structure in this research effort are active lamb wave and passive acoustic emission. The lamb wave technique is active because an input signal in the form of a wave is applied to a structure, the reflected signal from the defect and from the edges of the structure can be sensed from the piezoelectric sensors. Using information such as the wave speed and geometry of the structure, the location of the defect can be determined.

Acoustic emission can be defined as an acoustic wave generated from the release of strain energy due to defects in a material. An acoustic signal is the electrical signal generated from the sensor that responses to the acoustic wave [1, 19]. The acoustic emission technique is passive because the piezoelectric sensors on the structure are used to "listen" to the structure. If there is any defect on the structure, this acoustic emission signal would reflect the presence of the defect. Unlike the active lamb wave technique, the acoustic emission technique allows the detection of a defect, but not the exact location of the defect. Also, in order to generate the acoustic emission signal, the structure has to be under load such as a tensile load or bending load.

Acoustic emission can be generated from different types of material defects including fracture, plastic deformation, impact, friction and corrosive film rupture [4]. There are many methods that researchers use to utilize wave techniques and acoustic emission as a non-destructive health monitoring system. Some of these methods include [18, 19]

1) Pulse echo method – The time signal of output waves from sensors shows different peaks corresponding to reflection waves from a material defect or edges of structure. Based on the geometry of the structure and the arriving time of the wave signals, the location of the defect can be calculated. With the correct number of sensors used, the location of defect can be determined for 1-D or 2-D structures [9].

2) Differential signal method – The signal received from a damaged structure is used to subtract from a signal received from an identical but pristine structure. The result is the pure signal indicating the defect on the structure [10].

3) Zone location method – The signal received from a structure has different amplitudes corresponding to different defects. The highest amplitude signal corresponds to the defect that is closest to the sensor or the largest defect [19].

4) Correlation method – With an array of sensors, the signals received from these sensors will be correlated. A high level of correlation indicates a defect at the assumed site. A low level of correlation indicates the absence of a defect [19].

5) Electro-mechanical (E/M) impedance method – Each sensor has a radius of area in which if a crack is present within a sensor's area, the acoustic emission data from that sensor can detect the crack. Also, within a sensing area, the sensor's sensing ability also decreases as the distance of the defect increases from the sensor. The real part of the E/M impedance reflects the health of the structure [6].

6) Continuous sensor array (CSA) method – This is used in the passive acoustic emission technique. The CSA system uses an array of sensors to simultaneously detect the acoustic waves. Using parameters such as the geometry of the structure and signal amplitude, the structure defect can be determined [2].

The active lamb wave system uses an external excitation signal to excite the structure. This can be done with a signal generator. The passive acoustic emission system uses the defect from the structure as the source of wave. In a laboratory environment, defects can be introduced to a piece of test specimen using tensile test, compression test or fatigue test, etc. A popular method used to introduce defect to a test

structure is the pencil lead break method [17]. The pencil lead break method works when pressure is applied with a lead pencil on a structure until the lead breaks, this would create a mark that can be modeled as a crack on the structure.

Figures 2-9 and 2-10 demonstrate how the pulse echo method works. The data in Figure 2-10 is not a real data set, but a mock-up data to show how this method works.

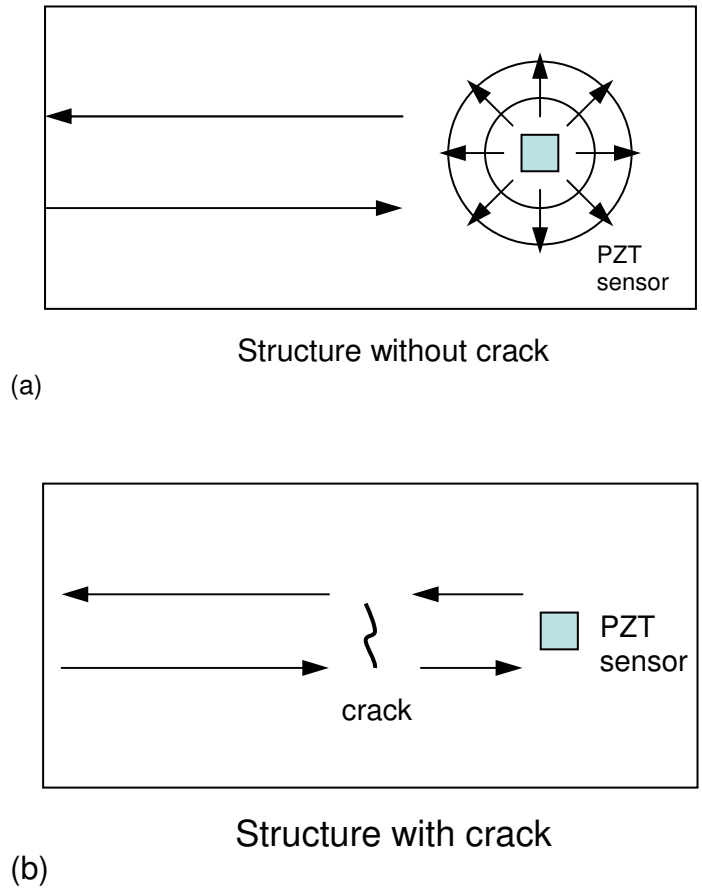

Figure 2-9. 1-D test structure with a piezoelectric sensor attached. The arrows represent the direction of wave propagation. (a) a structure without crack and (b) a structure with crack. The piezoelectric sensor acts as both actuator and transducer.

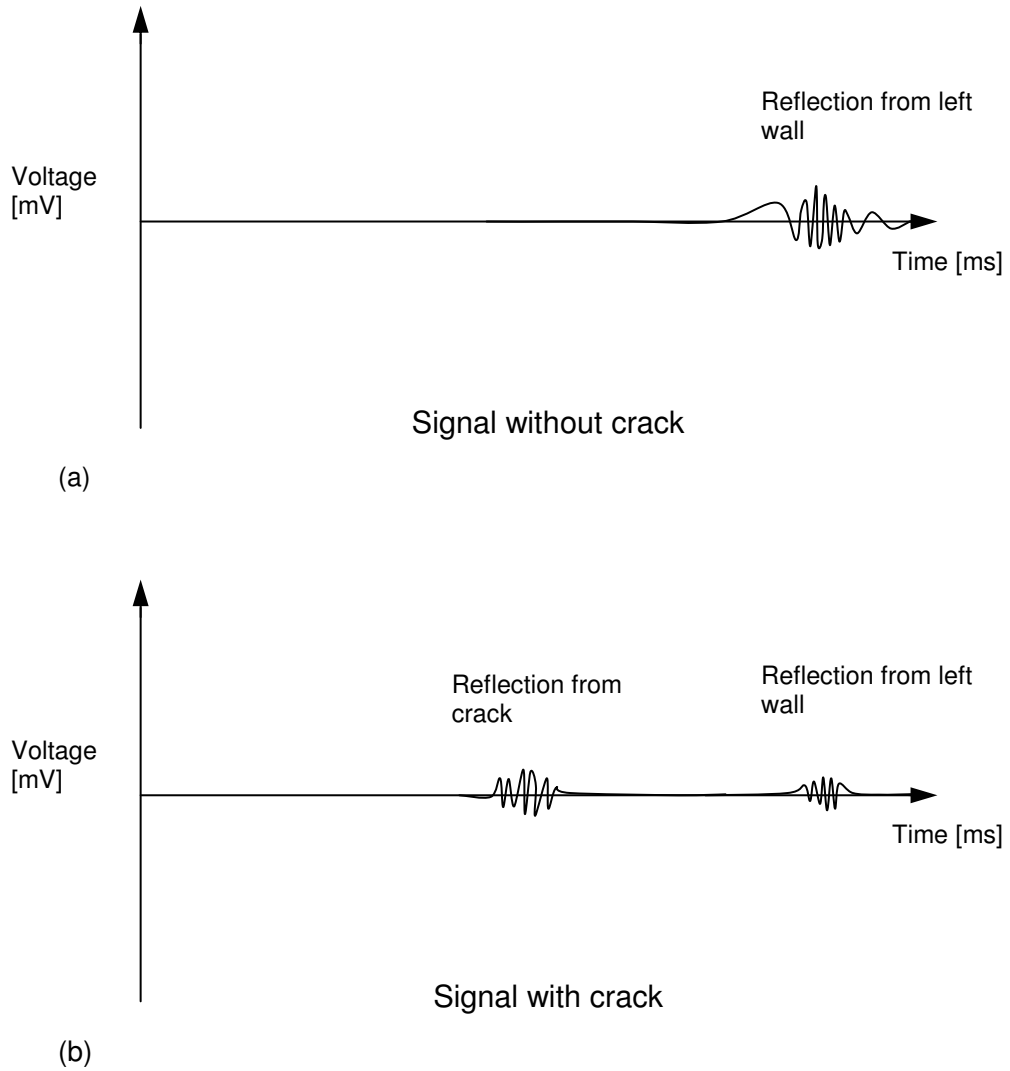

Figure 2-10. Mock-up wave signal of the test structure shown in Figure 2-9. (a) Wave signal shows the reflection from the left wall. (b) Wave signal shows the reflection from the crack and from the left wall [9].

3 Overview of Components Design and Operational Amplifier

The structural health monitoring (SHM) system uses piezoelectric sensors for generating and receiving signals from the structure. In order to successfully generate a signal into a structure and detect the reflected signal, some signal conditioning has to be implemented in order to capture the wave form. The main components that will be described in this thesis are charge amplifier, high pass filter, low pass filter and line driver. All of these components require the use of an active device, the operational amplifier, or op amp.

3.1 Overview of Components Design

Since the operating frequency range of Lamb wave is in the MHz range, these components have to operate to a frequency up to 2 MHz. This imposes a challenge in that as the operating frequency range of any op amp increases, its performance also decreases. This is a direct result of the gain-bandwidth (GBW) product. The concept of gain-bandwidth product of any op amp simply states that as the bandwidth increases, the open-loop gain of the op amp also decreases. Therefore, selecting the right op amp for the application is critical. This section briefly describes what each component does. Since all the component designs involve the use of op amps, a general review of op amp is given. The remaining sections will go also into detail of the design and testing of each component.

PZT sensors have very high output impedance. The input impedance of most measuring devices is not high enough to match the output impedance of the PZT sensors. The purpose of a charge amplifier is to provide a high input impedance to the incoming high impedance signal from the PZT sensor, while providing a low output impedance signal to a measuring device. This charge amplifier can be built using an op amp intended for this kind of application.

A high pass filter attenuates any low frequency content of a signal and only allows the higher frequency content to pass through. This is important because at very low frequency, the majority of the signal contents are noise. A high pass filter can be constructed using active device such as an op amp.

A low pass filter is the reverse of a high pass filter in that it attenuates the high frequency content and only allows the lower frequency content to pass through. This is also important because any frequency contents higher than the frequency of interest are not necessary to be included in the signal, and a low pass filter will also reduce the high frequency noise. This can also be built using an op amp. Therefore, a high pass filter combined with a low pass filter will form a band-pass filter.

In order to actuate a piezoelectric sensor, the input signal current must be high enough to actuate the sensor. The purpose of a line driver is to increase the current of the signal coming from a function generator into the piezoelectric sensor. A line driver is a device that will take the low current signal and drives it to a much higher current signal. The concept of a line driver is that it does not have a specific circuit configuration and the driver depends on the op amp output current itself. Therefore, the line driver can be any op amp circuit. In this application, the line driver circuit is built as a simple voltage amplifier to amplify the signal by a gain. Figure 3-1 summarizes how each component is connected with each other.

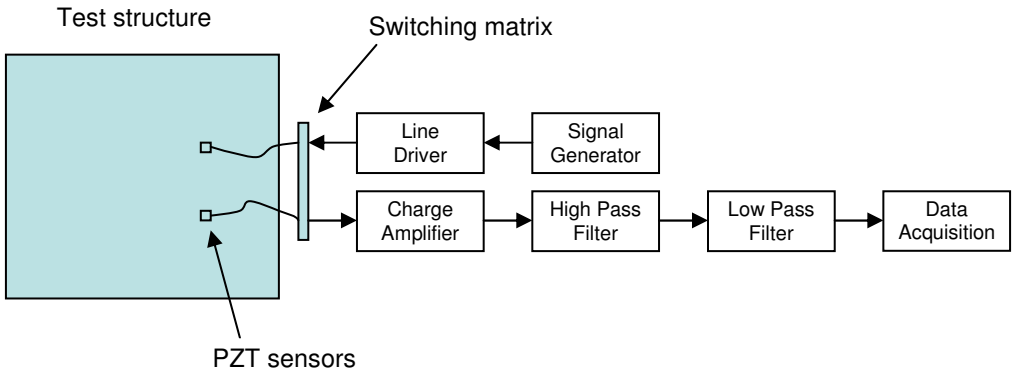

Figure 3-1. Overview of signal conditioning circuitry for sending a signal and receiving a signal from the PZT sensors.

In Figure 3-1, an input signal is applied to one of the two piezoelectric sensors. The other sensor detects the reflections of the input wave from both the defect (if present) and edges of the test structure. Using information such as the time it takes to detect a reflection wave and the geometry of the test structure, the location of a defect can be calculated. This is the pulse-echo method described in Section 2.3. The same analysis can be done on a pristine structure and a defected structure. Subtracting the signal of a defected structure from the signal of a pristine structure will show the reflection wave due to the defect. This is the differential signal method.

All of the op amps tested in this research are products of Analog Devices Inc. The main reason that op amps from Analog Devices Inc. were preferred over other manufacturers is because Analog Devices Inc. provides a PSpice circuit file for the majority of their products. This helps a great deal in the design process since the PSpice file for a particular op amp can be imported into PSpice and simulation can be run. This saved a tremendous amount of time in that not every single circuit needed to be built. A fast and easy simulation can be run in PSpice to see if the results are satisfactory. The PSpice demo version 9.2 [22] was used for the simulations. Although the demo version only allows 64 nodes, this is enough for most of the simulations ran since most of the circuits only require a few resistors and capacitors to run the simulation. The simulation results also resembled the actual physical circuit results quite closely.

Another reason for choosing op amps from Analog Devices Inc. is because they allow educational institutions to sample most of their products. This feature allows the flexibility to explore different op amps without having to purchase all of the products. Due to budget reason, this feature was very helpful since most of the op amps tested were samples.

Because most of the op amps tested are manufactured only in the surface mounted configuration (SOIC), prototyping became an issue since breadboard was used for building and testing circuits. Therefore, surface mount to DIP adapters were purchased from Accutek Microcircuit Corporation. These adapters were very easy to use and

inexpensive; on average, they cost about $5.00 US each. The op amps can be mounted on these adapters permanently using a regular soldering iron working under a microscope. These adapters saved lots of time because at the initial testing of the charge amplifier, wires were soldered directly onto the pins of the op amp chip. This led to very inconsistent results because firstly, pins can possibly have been soldered together and secondly, pins were broke off from the chip very easily. Figure 3-2 shows a picture of an op amp mounted on a SOIC to DIP adapter.

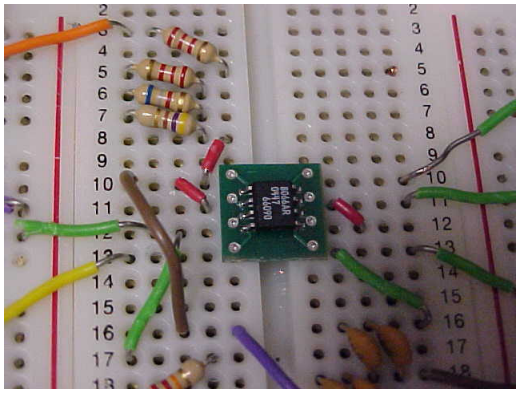

Figure 3-2. Picture showing an op amp mounted on a SOIC to DIP adapter for testing.

3.2 General Concept of Operational Amplifier

This section introduces the fundamental concepts of operational amplifier. It follows with an explanation of the ideal op amp using a simple amplifier example. This will show the reason of why high input impedance and low output impedance are desired, and thus the importance for the need of a charge amplifier. Although the information presented in the following sections may seem basic, it is important since all of the research work done were based on design and testing of op amp circuits.

An amplifier is a device that receives a signal, amplifies the signal and outputs the amplified signal. Many amplifiers used in modern electronics utilize a well known active device called the operational amplifier, abbreviated as op amp. With different circuit and op amp configurations, a variety of operations from the simple addition, subtraction and multiplication to the more complicated operations such as integration, differentiation and filtering can be performed. Figure 3-3 presents an op amp symbol and its internal circuit representation.

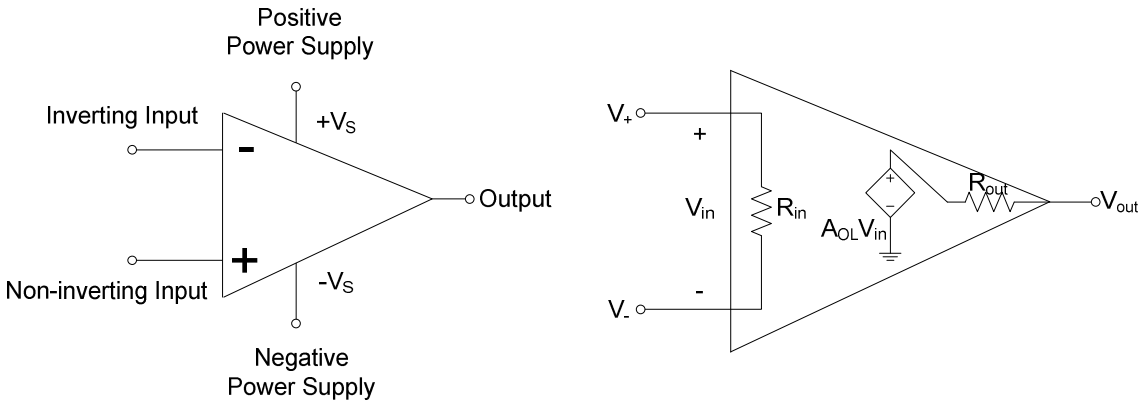

Figure 3-3. A typical op amp symbol. The left figure is the general representation. The right figure models the internal components of an op amp including the input and output impedances and the open-loop gain [5].

3.2.1 Ideal Op Amp

To fully understand the operation of op amps, one does not have to understand what components an op amp is consisted of. In fact, an op amp is consisted of hundreds of transistors that an understanding of the finest detail inside an op amp is not as important as an understanding on how to use an op amp to build and design a useful circuit.

To analysis an op amp circuit, one usually assumes the op amp to be the so-called "ideal" op amp. An ideal op amp is an op amp that has infinite open-loop gain, infinite input resistance, infinite bandwidth and zero output resistance. However, in practice, no op amps are truly ideal. The assumption of ideal op amp is a useful way to simplify the circuit analysis and the deviation of the actual op amp from the ideal op amp is usually small. A typical op amp can have open loop gain in the range of millions.

As stated above, an ideal op amp has infinite open-loop gain, input resistance, bandwidth and zero output resistance. Infinite bandwidth implies that the op amp performance is independent of the frequency of interest. This means that the op amp performance does not deteriorate with the frequency in which the op amp operates, regardless if it's zero frequency, DC, or high frequency in the MHz range. Infinite open-loop gain is desired because for a particular circuit configuration, a high open-loop gain would allow the output of the circuit to depend solely on the external circuit elements, but not the op amp itself. This is a huge flexibility in terms of design and testing of any circuits. To fully understand why an ideal op amp has infinite input resistance and zero output resistance, consider the simple amplifier demonstration shown in Figure 3-4.

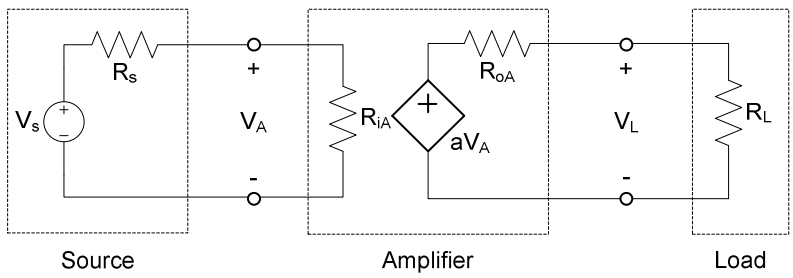

Figure 3-4. Simple amplifier model to demonstrate why an ideal op amp has infinite input resistance and zero output resistance [5].

The V_S and R_S are the voltage and internal resistance of the source, R_{iA} and R_{oA} are the input and output resistances of the amplifier respectively, a is the open loop gain for the amplifier, R_L is the load resistance. From the voltage divider principle,

$$V_A = \frac{R_{iA}}{R_S + R_{iA}} V_S \qquad and \qquad V_L = \frac{R_L}{R_{oA} + R_L} a V_A \tag{3.1}$$

The overall gain of the amplifier is defined as

$$\frac{V_L}{V_S} = a\left(\frac{R_{iA}}{R_S + R_{iA}}\right)\left(\frac{R_L}{R_{oA} + R_L}\right) \tag{3.2}$$

However, in order for the output signal to be amplified by the amplifier gain a without any voltage drop, the two quantities in parentheses must equal to a value of 1. This is true only if $R_{iA} \rightarrow \infty$ and $R_{oA} \rightarrow 0$. This is the exact reason why infinite input resistance and zero output resistance are desired.

Two very useful assumptions can be made when analyzing ideal op amps. These assumptions [20] can also be applied to real op amp with negligible errors. These are:

1) The current flowing into the input circuit is zero, $i_{in} = 0$.
2) The voltage at the inverting input is equal to the voltage at the non-inverting input, $V_n = V_p$.

4 Development of Charge Amplifier

A charge amplifier is a device connected to a piezoelectric sensor for signal conditioning purpose. The reason that a charge amplifier is needed is because piezoelectric sensors have very high output impedance. If this high output impedance is not matched with a high input impedance for the measuring device, the signal can hardly be detected. The idea is like having water running through a large pipe, if this large pipe is connected to a small pipe, it will restrict the water flow. This is the same idea that the output impedance of a sensor must be matched with the same input impedance of a device that is directly connected to the sensor.

The basic working principle of piezoelectric sensors is that if a force is applied to a piezoelectric material, it will generate a strain or displacement and in turn, it will generate an electric charge. Therefore, measuring the charge generated enables the measuring of the strain generated. Because current is a rate of change in charge, for simulation purposes, a piezoelectric sensor can either be modeled as a current source in parallel with a capacitor with value equal to the capacitance of the sensor [21], or as a voltage source in series with a capacitor with value equal to the capacitance of the sensor [23].

4.1 Various Charge Amplifier Configurations

Figure 5-1 depicts a simple charge amplifier with a piezoelectric sensor modeled as a voltage source in series with a capacitor.

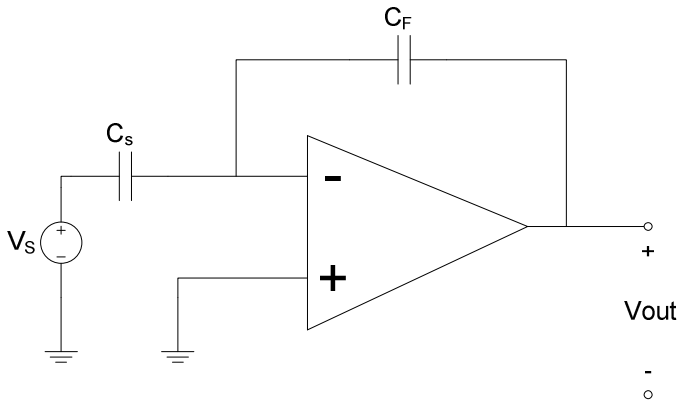

Figure 4-1. A simple charge amplifier with a piezoelectric sensor modeled as a voltage source in series with a capacitor [5].

In this circuit, V_S and C_S are the source voltage and capacitance, which are model of a piezoelectric sensor. C_F is a feedback capacitor that feeds the output current back into the inverting input of the op amp. Figure 4-2 presents this circuit with the direction of the current flows.

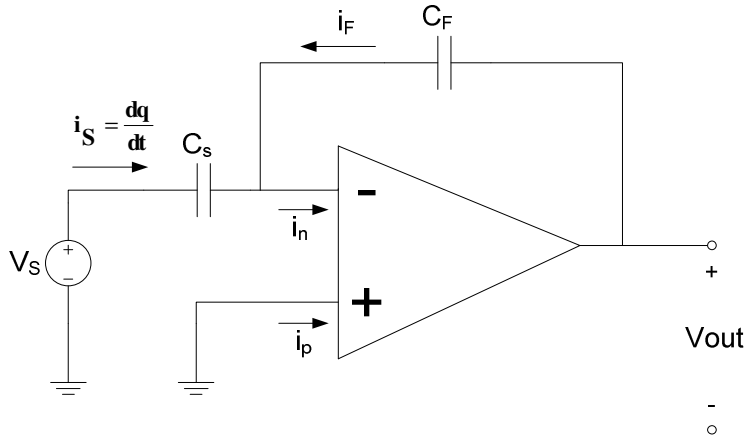

Figure 4-2. A simple charge amplifier shows the current flows. These currents are the current from the source, the feedback current and the currents at both the inverting and non-inverting terminals [20].

The current from the piezoelectric sensor is denoted as i_S. C_S is the capacitance of the sensor. To analysis this circuit, based on one of the two op amp assumptions from Section 3.2.1 that the current flowing into the input circuit is zero,

$$i_n = i_p = 0 \tag{4.1}$$

According to the Kirchoff's current law,

$$i_S + i_F = i_n \tag{4.2}$$

which leads to

$$i_S = -i_F \tag{4.3}$$

The output voltage can be written in terms of the feedback capacitance

$$V_{out} = \frac{1}{C_F}\int i_F \, dt = \frac{1}{C_F}\int -i_S \, dt = \frac{1}{C_F}\int -\frac{dq}{dt} dt = -\frac{q}{C_F} \tag{4.4}$$

This result states that the output voltage, V_{out}, depends only on the feedback capacitor, C_F, and not the input capacitance of the sensor nor the capacitance of the cable. Therefore, all the charges generated from the source will be converted into a change of voltage at the output, and then transferred to the feedback capacitor. This change of output voltage is $\Delta V_{out} = -\Delta Q / C_F$. This is a great advantage when the amplifier is being placed far away from the sensor through long cable connection. Since the output voltage is only dependent on the feedback capacitance, the stray capacitance from the cable will not come into place. A more practical charge amplifier is shown in Figure 4-3.

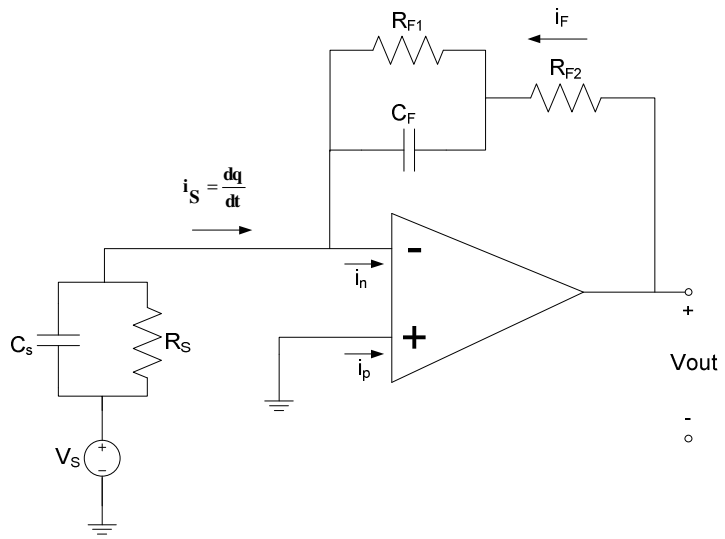

Figure 4-3. A more practical charge amplifier includes both feedback capacitor and feedback resistor. The piezoelectric sensor is modeled as a voltage source in series with a capacitor and resistor in parallel.

The charge amplifier in Figure 4-3 has a feedback resistor, R_{F1}, in parallel with C_F to avoid saturating C_F while charging C_F from the source. There is also an optional second feedback resistor, R_{F2} in series with the C_F and R_{F1} parallel combination. The purpose of R_{F2} is to provide a minimum output impedance to the charge amplifier throughout the whole frequency spectrum. This is because a capacitor is virtually a short circuit at high frequency, all the currents will run through the C_F path instead of the R_{F1} path at high frequency, R_{F2} avoids shorting the feedback path. Since low output impedance is desired from this circuit, the value of R_{F2} is kept at very low value around 100 Ω. In addition to R_{F1} and R_{F2}, a source resistor, R_S, should be placed in parallel with the source capacitor, C_S. The purpose of this resistor is to model the piezoelectric sensor with a more practical model. A capacitor, C_C, modeled as the capacitance of the connection wires can also be put in parallel with the piezoelectric sensor to achieve a more realistic model.

Another charge amplifier configuration is high impedance voltage follower with gain [13]. This configuration is a non-inverting amplifier and is shown in Figure 4-4.

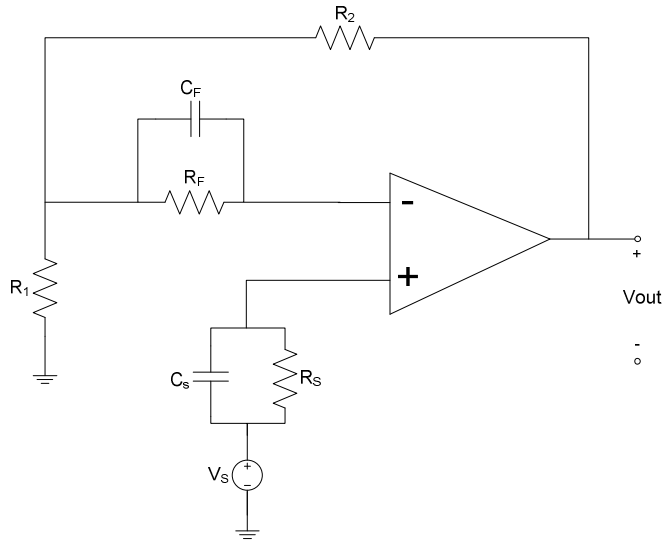

Figure 4-4. A charge amplifier modeled as a high impedance voltage follower with gain is a non-inverting amplifier [13].

In Figure 4-4, the series and parallel combination of C_S, R_S and V_S are the model for the piezoelectric sensor. Note that for this configuration, the sensor model is connected to the non-inverting terminal instead of the inverting terminal as in Figure 4-3. The parallel combination of C_F and R_F are the feedback path. Again, all the charges from the source are transferred to the feedback capacitor C_F. The advantage of this configuration is that a gain can be applied and the gain is solely determined from the external resistors. This gain [13] is determined as

$$gain = 1 + \frac{R_2}{R_1} \tag{4.5}$$

4.2 Piezoelectric Sensor Impedance Calculation

Since the main purpose of a charge amplifier is to convert a high impedance signal to a low impedance signal, this section briefly introduces the concept of impedance and how it can be calculated using a mathematical model. In real life, the impedance of a circuit can often be measured. This section gives a general overview of how the impedance can be approximated using mathematical formulas and how it can change with frequency.

Throughout the simulation and design process, the piezoelectric sensor was modeled as a voltage source in series with a capacitor and resistor parallel combination. A voltage source was easily obtained from a function generator. The proper resistance and capacitance values were chosen to match the output impedance given on the specification of the piezoelectric sensors. The output impedance of a piezoelectric sensor can be calculated according to the simple formulas of impedances for resistors and capacitors.

$$Resistance: \quad V_R = iR \quad \rightarrow \quad Z_R = R \tag{4.6}$$

$$Capacitance: \quad V(t) = \frac{1}{C}\int_{t_0}^{t_f} i(t)dt \quad \rightarrow \quad V_C = Z_C i_C \quad \rightarrow \quad Z_C = \frac{1}{sC} \tag{4.7}$$

For equivalent impedances in series and in parallel calculation, the following rules apply.

For impedance in series: $$Z_{eq} = Z_1 + Z_2 + Z_3 + \ldots\ldots \tag{4.8}$$

For impedance in parallel: $$\frac{1}{Z_{eq}} = \frac{1}{Z_1} + \frac{1}{Z_2} + \frac{1}{Z_3} + \ldots\ldots \tag{4.9}$$

Therefore, for the piezoelectric sensor modeled as a voltage source in series with a capacitor and resistor parallel combination as shown in Figures 4-3 and 4-4, the equivalent impedance can be calculated according to these general rules.

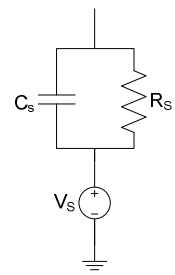

$$\frac{1}{Z_{eq}} = \frac{1}{Z_{Rs}} + \frac{1}{Z_{Cs}} = \frac{1}{R_S} + \frac{1}{1/sC_S} = \frac{1 + jwC_S R_S}{R_S}$$

The equivalent impedance for the piezoelectric sensor is then

$$Z_{eq} = \frac{R_S}{1 + jwC_S R_S} \tag{4.10}$$

The resistance and capacitance values given from the specification of the sensors are R_S = 100 kΩ and C_S = 2.82 nF. Using equation 4.10, the output impedance of the model at low frequency such as 10 Hz is calculated as

$$Z_{eq} = \frac{R_S}{1 + jwC_S R_S} = \frac{100 \times 10^3\,\Omega}{1 + j(10\,Hz)(2\pi)(2.82 \times 10^{-9}\,F)(100 \times 10^3\,\Omega)} = 99984 \angle -0.018\,\Omega$$

The result shown is converted from imaginary number to magnitude and degree in radian. At high frequency such as at 2 MHz, the impedance is

$$Z_{eq} = \frac{R_S}{1 + jwC_S R_S} = \frac{100 \times 10^3\,\Omega}{1 + j(2 \times 10^6\,Hz)(2\pi)(2.82 \times 10^{-9}\,F)(100 \times 10^3\,\Omega)} = 28.2 \angle -1.57\,\Omega$$

As shown, the output impedance drastically decreases as frequency increases. This is due to the fact that at high frequency, the capacitor behaves as a short circuit and all the current will go through this path instead of the resistor path, creating a virtual short circuit. Thus the impedance becomes much lower at high frequency.

The same analysis can be carried out for the feedback path of the charge amplifier. The impedance of the feedback path determines the output impedance of the charge amplifier.

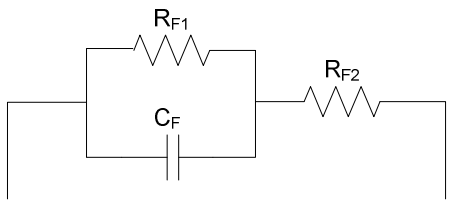

According to equation 4.10, the equivalent impedance for a resistor and capacitor in parallel is calculated as in equation 4.10. The overall equivalent impedance for the feedback path is therefore

$$Z_{eq} = \frac{R_{F1}}{1 + jwC_F R_{F1}} + R_{F2} \tag{4.11}$$

As equations 4.10 and 4.11 show, the effective impedance of both the piezoelectric sensor and the feedback path decreases as frequency increases.

4.3 Specification of Op Amp Used

All of the operational amplifiers used in this research are manufactured from Analog Devices Inc. As stated before, the two main reasons for using products from Analog Devices Inc. is because the PSpice circuit files provided for most of their products and the sampling option they offer. The op amp used for the charge amplifier is the AD745. The AD745 is a low voltage and low current noise, high speed FET operational amplifier. It has a very high input impedance of 10 GΩ / 20 pF that is much higher than a typical op amp such as the μA741, which has an input impedance of 2 MΩ / 1.4 pF [5]. From Section 4.2, the impedance for the AD745 can be calculated from equation 4.10.

At frequency 10 Hz,

$$Z_{eq} = \frac{R}{1 + jwCR} = \frac{10\times10^{9}\,\Omega}{1 + j(10Hz)(2\pi)(20\times10^{-12}\,F)(10\times10^{9}\,\Omega)} = 793\times10^{9}\angle -1.49\,\Omega$$

At frequency 2 MHz,

$$Z_{eq} = \frac{R}{1 + jwCR} = \frac{10\times10^{9}\,\Omega}{1 + j(2\times10^{6}\,Hz)(2\pi)(20\times10^{-12}\,F)(10\times10^{9}\,\Omega)} = 3979\angle -1.57\,\Omega$$

Section 3.2.1 equation 3.2 stated that the quantity $\left(\frac{R_{iA}}{R_S + R_{iA}}\right)$ needs to be as close to one as possible. Using the magnitudes of the input impedance of the AD745 and the impedance of the piezoelectric sensor calculated from Section 4.2:

At frequency of 10 Hz,

$$\left(\frac{Z_{iA}}{Z_S + Z_{iA}}\right) = \left(\frac{793\times10^{9}}{99984 + 793\times10^{9}}\right) = 0.99$$

At frequency of 2 MHz,

$$\left(\frac{Z_{iA}}{Z_S + Z_{iA}}\right) = \left(\frac{3979}{28.2 + 3979}\right) = 0.99$$

These results show that at both high and low frequencies, the input impedance of the AD745 is much higher than the impedance of the sensor. This closely matches the ideal op amp assumption with very negligible error.

The AD745 also has a gain bandwidth product of 20 MHz. At a frequency of 2 MHz, which is the upper frequency of interest in this application, the open-loop gain is almost 20 dB. These and among other characteristics make the AD745 an ideal choice for the charge amplifier.

There are five different grades for the AD745, the AD745J was chosen because the other grades are rated at a larger operating temperature range for military purposes. Some of these are not available for sampling. A PSpice circuit file, ad745j_cir, was downloaded from the Analog Devices Inc. website for modeling purpose.

The data sheet of the AD745 offers two configurations on how to build a charge amplifier. These two configurations were shown in Figures 4-3 and 4-4. The configuration in Figure 4-3 is the more common type of charge amplifier over the voltage follower configuration in Figure 4-4. Both of these circuits were simulated in PSpice, built and tested. The following sections present the results.

The circuit files downloaded from the website cannot be immediately imported into PSpice. A few extra steps have to be taken before the file will work. A good amount of time was spent to find out how to get the downloaded circuit file to work successfully, therefore, these steps are outlined in Appendix A.

4.4 PSpice Simulation

Several simulations were performed on the AD745 using the circuit file Analog Devices Inc. provided. Different parameters were used to try to obtain the best result. These designs were also built, tested and compared with the simulation results. Although there are unaccountable issues with building circuits on breadboard; for the most part, the PSpice simulation results resemble the actual circuit results quite closely. For all the simulations in this section, the piezoelectric sensor was modeled according to Section 4.2. Using the method described in Appendix A, a symbol for the op amp can be obtained from the downloaded circuit file. Figure 4-5 shows this pictorial representation of an op amp in PSpice in comparison with a familiar op amp symbol.

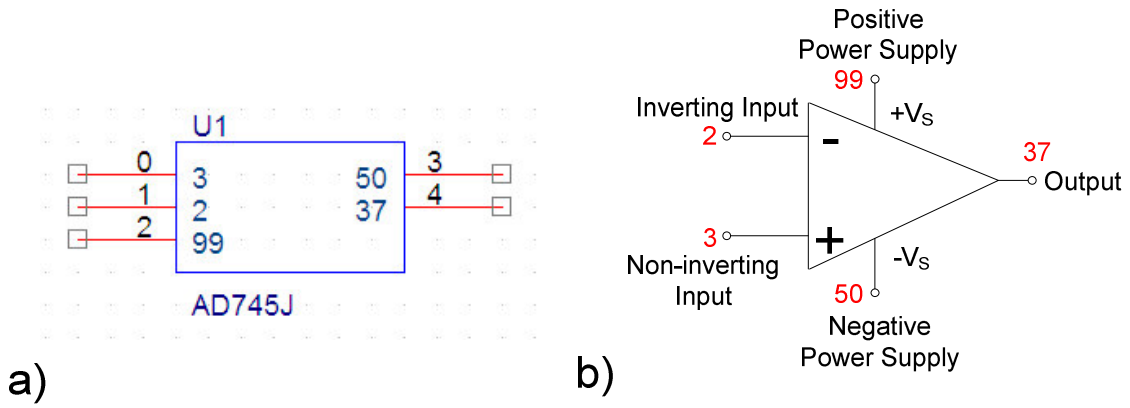

Figure 4-5. a) PSpice representation of an op amp. The pin numbers 3, 2, 99, 50, 37 correspond to the five pins shown in b). b) A familiar op amp representation shows the two inputs, two power supplies and one output.

4.4.1 Simulation 1 – Inverting Charge Amplifier

The first simulation performed was the typical inverting charge amplifier configuration shown in Figure 4-3, which is repeated here for ease of comparison to the PSpice schematic.

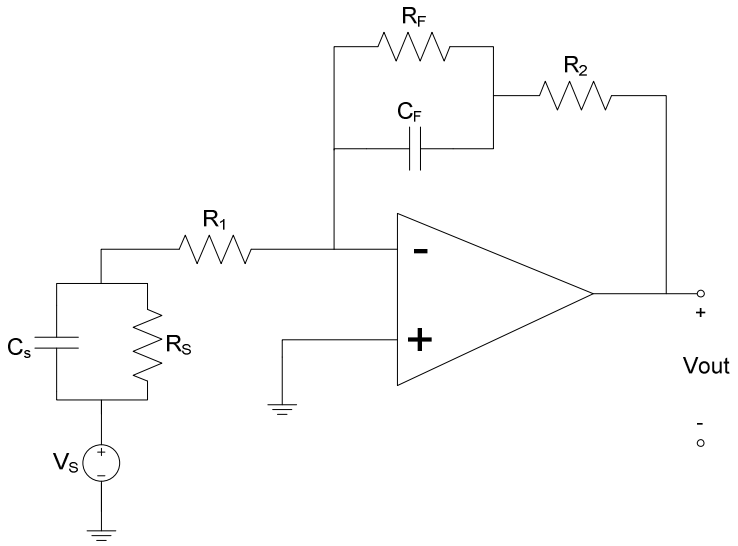

Figure 4-6. Inverting charge amplifier configuration.

The resistance and capacitance values for the PSpice model were set to the specification of the piezoelectric sensor used, which was stated in Section 4.2. These values are R_S = 100 kΩ and C_S = 2.82 nF. The feedback resistance and capacitance values were set to the same values as the source resistance and capacitance, so there will be a gain of 1. Therefore, for initial testing, R_F = 100 kΩ and C_F = 2.82 nF. Also, R_2 was set to 10 Ω for the first simulation. An optional low value resistor R_1 is added for the same purpose as R_2 as stated in Section 4.1. Figure 4-7 shows the PSpice schematic and Figure 4-8 shows the simulation result from 1 Hz to 10 MHz and physical circuit results. The simulation was obtained using the AC Sweep/Noise option in the simulation setting.

A function generator and an oscilloscope were used for testing the actual circuit. A range of input frequencies were applied to the circuit, the output voltage at each frequency was estimated from the oscilloscope. Due to the rough approximation of reading the output voltage from an oscilloscope and the inconsistence with breadboard, a

significant amount of errors can be introduced in the experimental results. Nevertheless, the results should be much more consistent and cleaner from noise with PCB board.

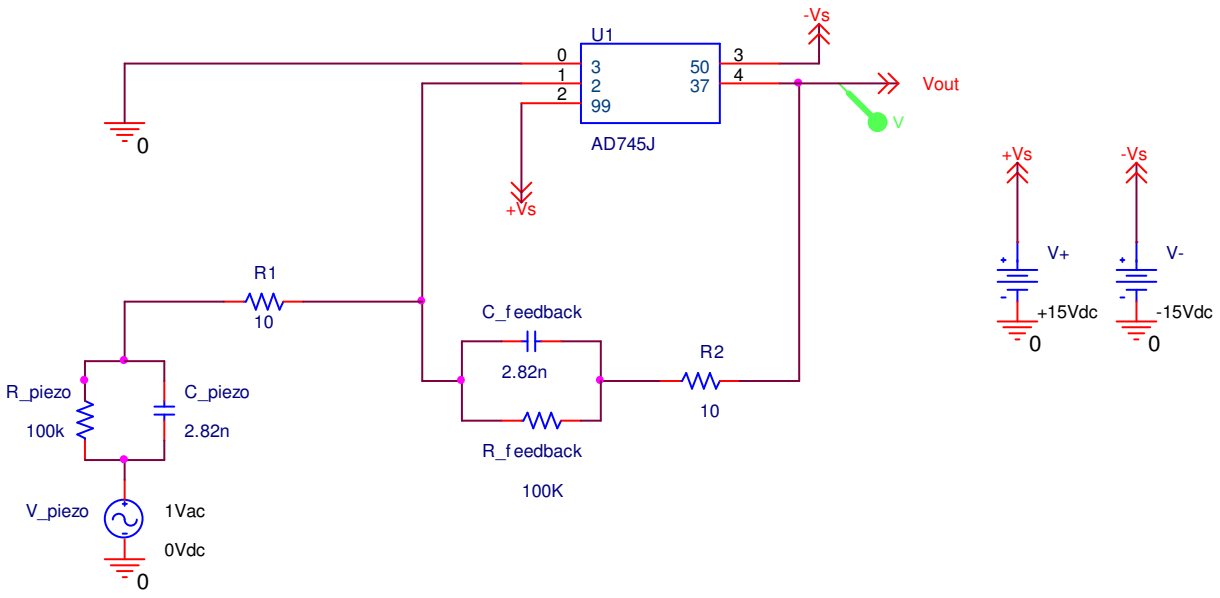

Figure 4-7. PSpice model for the inverting charge amplifier shown in Figure 4-6.

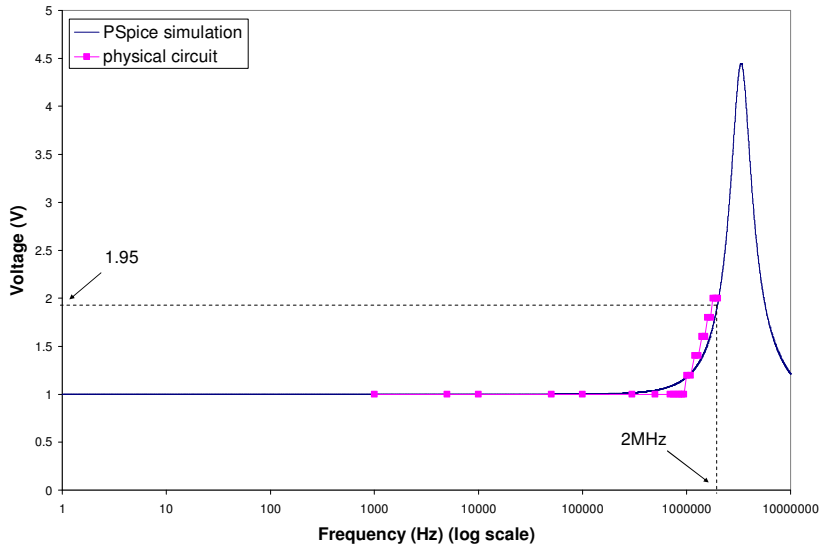

Figure 4-8. PSpice simulation and physical circuit results for inverting charge amplifier.

For a charge amplifier, the ideal response is a flat response throughout the frequency range of interest, in this case, from 0 Hz (DC) to 2 MHz. However, Figure 4-8 clearly shows that at 2 MHz, the response is at 1.95 V. At around 3 MHz, the response spikes to a voltage of 4.5V. Even though the frequency of interest for this application is only up to 2 MHz, one can claim that using a low pass filter will cutoff the frequency content beyond 2 MHz and the circuit will work fine. While this is true, a careful inspection of Figure 4-8 shows that the response starts to rise well before 2 MHz.

This spike was the biggest challenge in the design process of the circuit. Different parameters and configurations were tried, built and tested many times. Efforts were tried to move the spike to higher frequency so that the response would not rise up as early as shown in Figure 4-8. But this created other unexpected problems. One such problem was that much higher spikes were observed at the response. As the magnitude of the spike becomes higher, the response would also starts to rise up at earlier frequency. Figure 4-9 shows a response for setting R_2 = 100 Ω and everything else the same.

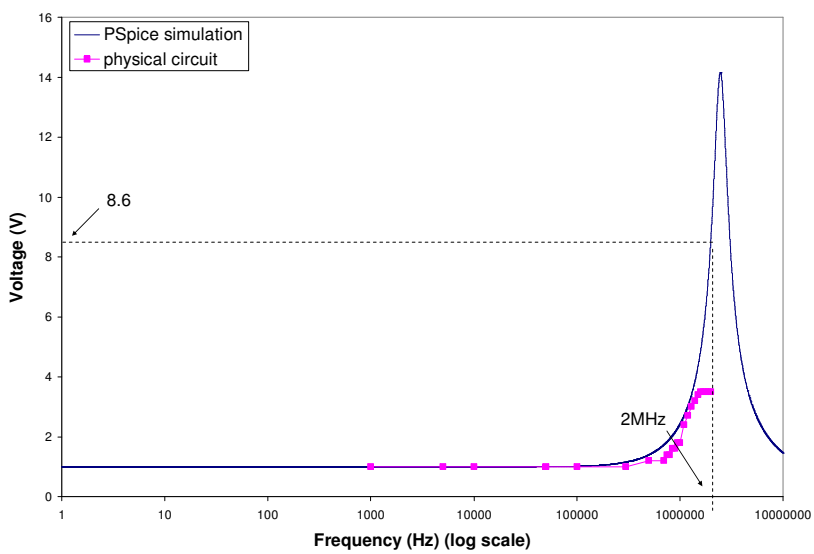

Figure 4-9. Response of inverting charge amplifier with R_2 = 100 Ω shows a spike more than twice as large as in response shown in Figure 4-8. The response rises up to 8.6 V at 2 MHz.

This unexpected spike is a direct result of an extra pole in the transfer function in the op amp. The transfer function for the circuit in Figure 4-7 can be calculated as below.

$$TF = \frac{Z_{feedback}}{Z_{input}} = \frac{\dfrac{R_S}{R_S C_S s + 1} + R_1}{\dfrac{R_F}{R_F C_F s + 1} + R_2} = \frac{\dfrac{R_S + R_1(R_S C_S s + 1)}{R_S C_S s + 1}}{\dfrac{R_F + R_2(R_F C_F s + 1)}{R_F C_F s + 1}} = \frac{\left(R_S + R_1(R_S C_S s + 1)\right)\left(R_F C_F s + 1\right)}{\left(R_S C_S s + 1\right)\left(R_F + R_2(R_F C_F s + 1)\right)}$$

Since $R_S = R_F$ and $C_S = C_F$, the transfer function can be simplified as

$$TF = \frac{R_S + R_1(R_S C_S s + 1)}{R_F + R_2(R_F C_F s + 1)} = \frac{R_S + R_1(R_S C_S s + 1)}{R_S + R_2(R_S C_S s + 1)} = \frac{R_1 R_S C_S s + R_S + R_1}{R_2 R_S C_S s + R_S + R_2}$$

which has one pole and one zero depending on the values of R_1 and R_2. Inspection of the transfer function shows that if $R_1 = R_2$, the denominator and numerator of the transfer function are the same and therefore, the transfer function would become 1 with the pole and zero canceling each other. In other word, the response should be flat with a gain of 1 for a frequency range all the way up to the bandwidth of the op amp, which is 20 MHz for the AD745. However, Figure 4-8 clearly shows that this is not the case. There is an extra pole in the transfer function from the op amp that is affecting the overall response. This extra pole cannot be accounted for since the circuit analysis is what can be controlled, but not the op amp imperfection. Therefore, after several weeks of trimming and fine-tuning of the circuit, it was decided to move forward to try a different configuration. This configuration was the high impedance voltage follower circuit shown in Figure 4-4 and is presented in the following section.

4.4.2 Simulation 2 – High Impedance Voltage Follower Charge Amplifier

The circuit used in this simulation is the high impedance voltage follower shown in Figure 4-4, which is repeated here for ease of comparison to the PSpice schematic.

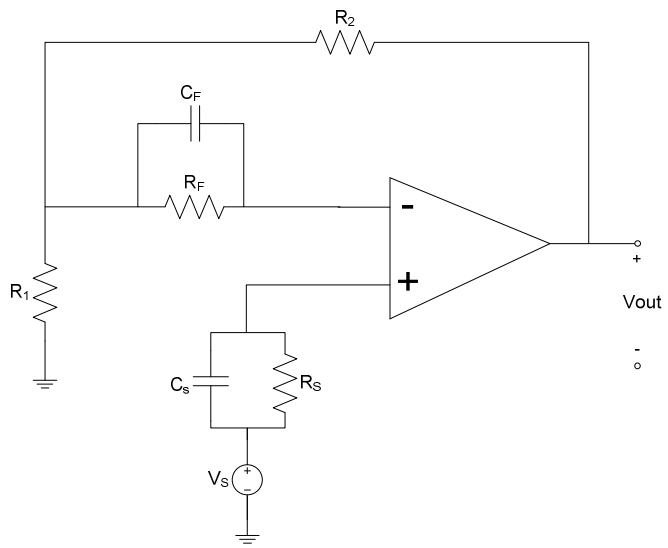

Figure 4-10. A noninverting charge amplifier configuration is modeled as a high impedance voltage follower [14].

The gain of this circuit is

$$gain = 1 + \frac{R_2}{R_1}$$

For the PSpice simulation, the resistance and capacitance of the piezoelectric sensor are modeled as described in Section 4.2 with R_S = 100 kΩ and C_S = 2.82 nF. The feedback resistance and capacitance values are also set to be the same as the sensor values, that is R_F = 100 kΩ and C_F = 2.82 nF. The R_1 and R_2 values are set to be equal, therefore, the response should be flat at 2 V. Figures 4-11 shows the PSpice schematic.

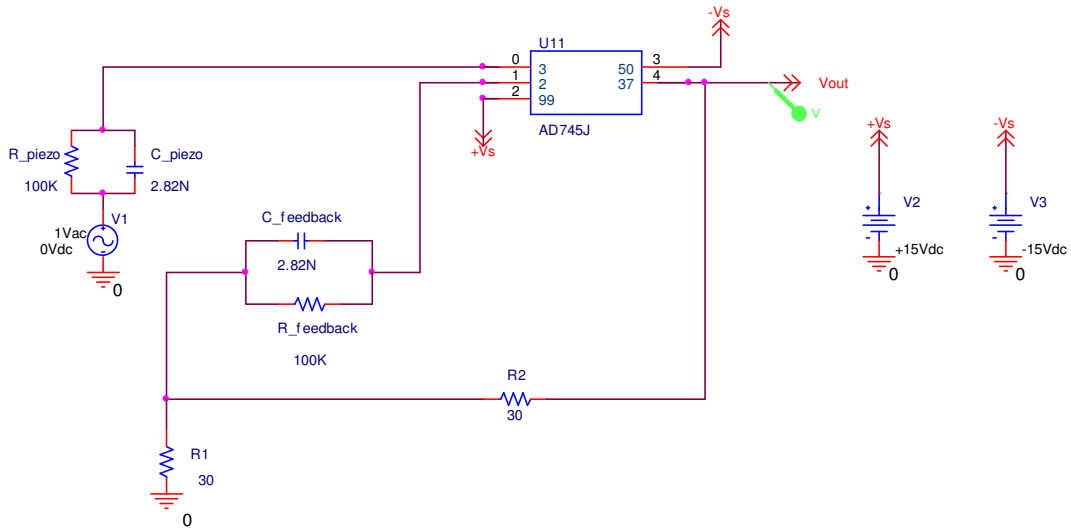

Figure 4-11. PSpice model for the high impedance voltage follower charge amplifier.

After a few simulations of this circuit, it was found that the same problem with the extra pole existed for this high impedance voltage follower charge amplifier configuration. However, the effect of this extra pole is not as large as the effect on the configuration described in the previous circuit. Figure 4-12 shows the simulation result for the circuit in Figure 4-11 from DC to 10 MHz and the physical circuit result for a range of frequencies. Figure 4-13 shows the same simulation result from DC to 2 MHz.

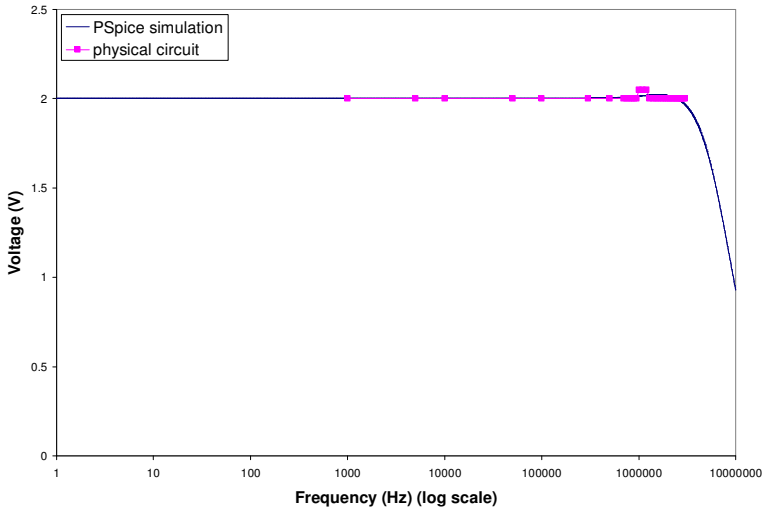

Figure 4-12. PSpice simulation and physical circuit results for high impedance voltage follower charge amplifier.

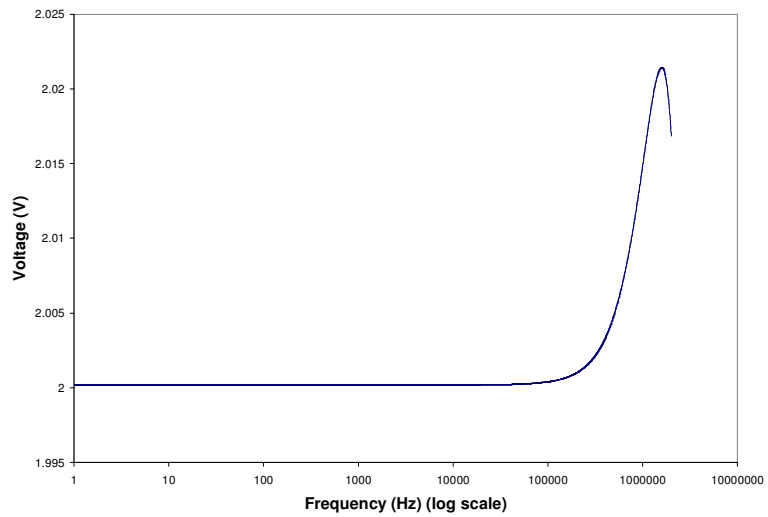

Figure 4-13. Response in Figure 4-12 from DC to 2 MHz shows that the response only spikes up to 2.02 V.

It was found that the values of R_1 and R_2 are the determining factor for a flat response. With the existence of the unknown extra pole in the op amp, it was quite difficult to obtain a perfectly flat response; therefore, a compromise had to be established. It was also found that if the values of R_1 and R_2 are too high, the response would spike up to a higher voltage and thus the response would rise up; if the values of R_1 and R_2 are too low, the response would start rolling off before 2 MHz, which is not acceptable either. Therefore, after a few trial and error, it was found that setting R_1 and R_2 to be 30 Ω is the best compromise. This would result in a gain of 2 and a fairly flat response for the output.

It was also found that setting $R_1 = 150\ \Omega$ and $R_2 = 600\ \Omega$ would result in a fairly flat response with a gain of 5. This simulation result is shown in Figure 4-14 from DC to 10 MHz. The same response from DC to 2 MHz is shown in Figure 4-15. This is an easier circuit to build since the resistance values are not extremely low and the tolerance of resistors are not as critical as if $R_1 = 30\ \Omega$ and $R_2 = 30\ \Omega$. Also, a gain of 5 would strengthen the signal to noise ratio of the output.

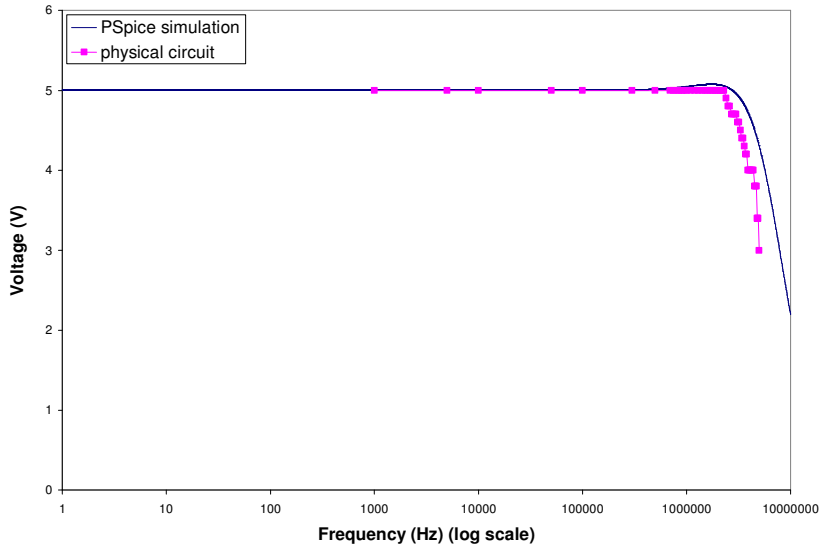

Figure 4-14. PSpice simulation response of high impedance voltage follower charge amplifier with $R_1 = 150\ \Omega$ and $R_2 = 600\ \Omega$ resulting a gain of 5.

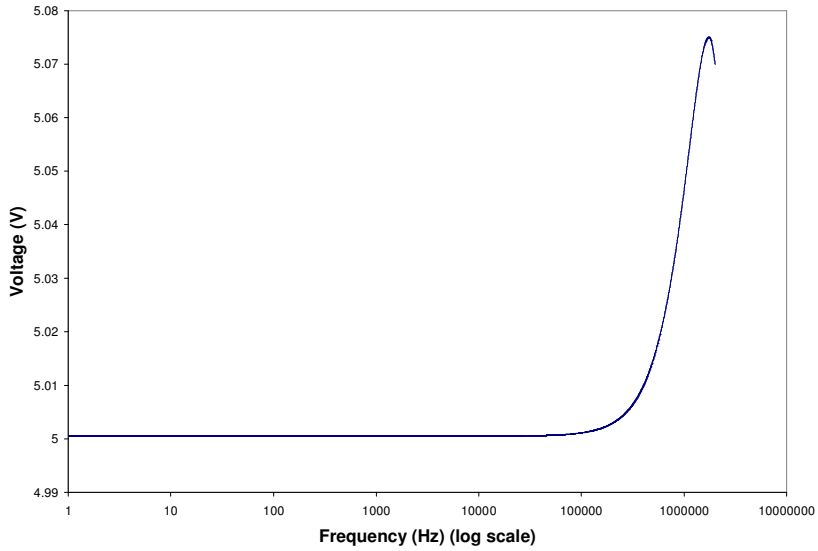

Figure 4-15. Response in Figure 4-14 from DC to 2 MHz shows that the response only spikes up to 5.07 V.

This section described the different characteristics and the need for a charge amplifier for piezoelectric sensors. Two different types of circuit were explored and simulated using PSpice for the charge amplifier configuration. These two circuits were shown in Figures 4-6 and 4-10. The first one is a typical inverting charge amplifier configuration, which is well known and well documented in most electronics textbooks. The second configuration, a high impedance voltage follower, is a less familiar version of a charge amplifier. While both circuits would work for the application at hand, which has a frequency range of interest from DC to 2 MHz, the voltage follower configuration showed a flatter response, which is what we aim for. Since the main purpose of a charge amplifier is to bring a high impedance signal from a piezoelectric sensor to a low impedance signal, both circuits can achieve this goal.

The problem with the extra pole in the transfer function of the op amp AD745 was unexpected. This extra pole created the biggest issue in the design process since not knowing the exact location of the pole makes it very difficult to try to compensate for it. Therefore, different trials were simulated to find the best compromise.

PSpice reduced the design process time tremendously in terms of building circuit. A few circuits were built at the beginning of the design phase and were compared to the PSpice simulation results. Given the errors involved in reading the output voltage from an oscilloscope and the inconsistence of breadboard, it was found that the actual physical circuit performance follows the PSpice results quite closely. Therefore, in the later half of the design process, PSpice was mainly used. Once a possible “good” design was determined, the actual circuit was built and tested. This saved a tremendous amount of time and effort since a good deal of time was spent on trial and error.

5 Development of High Pass Filter

A high pass filter is used to attenuate the low frequency content of a signal and allow only the high frequency content of the signal to pass through. The most common high pass filter is the Sallen-Key high pass filter. The Sallen-Key configuration is the most common type of filter, it is well documented in most textbooks and it is easy to build using off-the-shelf components. It requires one op amp, two resistors and two capacitors for each stage. Matching components can be used so that the variation of component tolerance is minimized. The response of a Sallen-Key filter does not exhibit ripples in the pass-band and stop-band such as a Chebyshev or Elliptic filter does.

The Sallen-Key configuration is a second order active filter, which rolls off the unwanted frequency content in the stop-band at 40 dB per decade. High order filters can be built by cascading two or more second order filters together. Typically speaking, the higher the order, the steeper the roll off will be. Figure 5-1 presents the Sallen-Key high pass filter circuit.

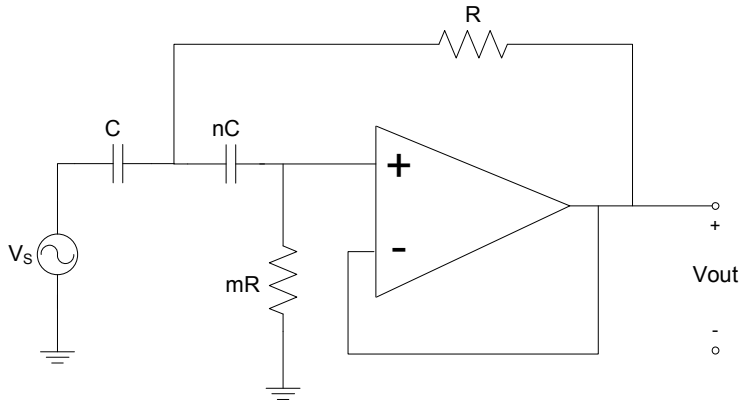

Figure 5-1. Sallen-Key second order high pass filter [5].

The transfer function for the high pass filter looks like

$$TF = \frac{-(f/f_0)^2}{1-(f/f_0)^2 + (j/Q)(f/f_0)} \tag{5.1}$$

where f is frequency normalized to f_0, f_0 is the cutoff frequency and Q is a parameter that determines the output response. Both f_0 and Q can be defined as

$$f_0 = \frac{1}{2\pi\sqrt{mn}RC} \tag{5.2}$$

and

$$Q = \frac{\sqrt{mn}}{n+1} \tag{5.3}$$

In general, the value of Q can range from 0.2 to 100, with values near unity being the most common. A common value for Q is 0.707, which is the lowest Q value before the response starts peaking. Figure 5-2 shows the magnitude plot for a standard high pass filter. As can be seen in Figure 5-2, any Q values above 0.707 would result in peaking in the response.

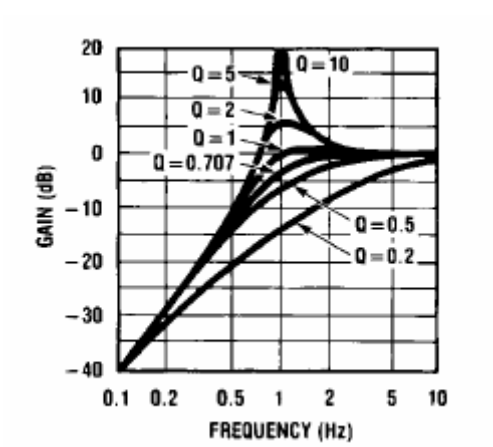

Figure 5-2. Magnitude plot for a typical second order high pass filter [15].

As indicated in Figure 5-1, the design process of a high pass filter includes choosing the Q value and picking out the resistor and capacitor values. Analog Devices Inc. offers a very easy to use interactive filter design on their website. It is called "Interactive Design Tools: Op Amps: Active Filter Synthesis [11]". The user needs to input information such as the type of filter, the order of the filter, the cutoff frequency and the number of stages, the Design Tools would generate the R and C values. The design of the high pass filter in this research came from this Design Tool from Analog Devices Inc. There is also a fairly straightforward step by step design by hand procedure from Franco [5]. This design procedure method was also explored to compare the design to the one from Analog Devices Inc.'s online Design Tool.

5.1 Selection of Op Amps and Design Parameters

The initial design of the high pass filter is a second order Butterworth Sallen-Key circuit with a cutoff frequency of 50 kHz and a $Q = 0.707$. The initial op amp selected for this high pass filter was the AD8129. However, this op amp is a differential receiver amplifier and its applications are differential line receiver and instrumentation amplifier, not active filtering. Also, we seemed to have problem with the gain-bandwidth product because we were not getting the bandwidth that we needed, even though it's rated at 200 MHz. Therefore, a different op amp, the AD8066, was selected. The AD8066 is a high performance, fast FET input amplifier with a bandwidth of 145 MHz at an open-loop gain of -3dB. Its applications include instrumentation and filtering. Therefore, the AD8066 is a good fit for use of a high pass filter.

As the same as the charge amplifier, PSpice was used for simulation of the high pass filter. Resulting circuits from PSpice were built, tested on a breadboard to compare with the simulation result. The physical circuit results resemble the PSpice results quite closely.

5.2 High Pass Filter Design from Analog Devices Inc.

The design from Analog Devices Inc.'s Interactive Design Tools: Op Amps: Active Filter Synthesis has the parameters shown in Figure 5-3. This is a second order Butterworth Sallen-Key high pass filter with a cutoff frequency of 50 kHz and a *Q* value of 0.707.

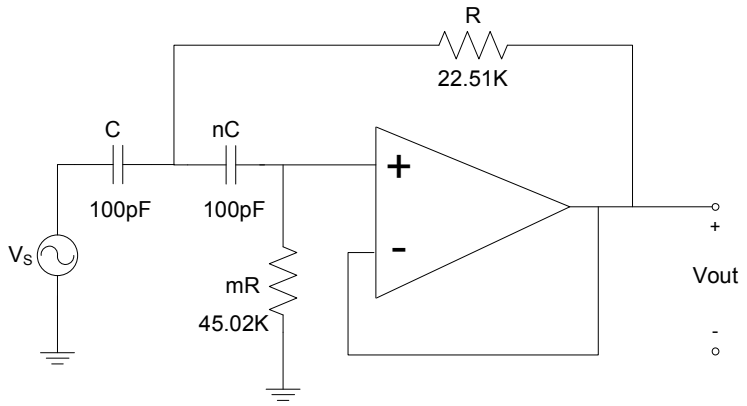

Figure 5-3. Second order high pass filter from Analog Devices Inc.'s Design Tool with a cutoff frequency of 50 kHz and a Q value of 0.707 [11].

5.3 High Pass Filter Design Step by Step Procedure

The design procedure offered from Franco [5] has the following procedures to design a high pass filter. This procedure follows the circuit shown in Figure 5-1 and is as follow:

1) Specify the cutoff frequency f_0 and Q.
2) Use equal capacitors for C and nC (n = 1) and determine the required value of m to achieve the given Q using equation 5.3.
3) Select a proper pair of resistors in the kΩ to satisfy the ratio from 1).
4) Use equation 5.2 to calculate capacitance C and select the closest standard capacitor values.
5) Use equation 5.2 to recomputed R and select the closest standard resistor values for R and mR.

Using the above procedures with a cutoff frequency of 50 kHz and a Q of 0.707 and if selecting C = 100 pF and R = 22.51 kΩ:

1) f_0 = 50 kHz and Q = 0.707

2) Select C = 100 pF and n = 1 and use equation 5.2

$$Q = \frac{\sqrt{mn}}{n+1} \qquad \rightarrow \qquad m = \frac{(Q(n+1))^2}{n} = \frac{(0.707(1+1))^2}{1} = 2$$

3) Select R = 22.51 kΩ and mR = 45.02 kΩ

4) Use equation 5.2

$$f_0 = \frac{1}{2\pi\sqrt{mn}RC} \qquad \rightarrow \qquad C = \frac{1}{2\pi\sqrt{mn}Rf_0}$$

and

$$C = \frac{1}{2\pi\sqrt{mn}Rf_0} = \frac{1}{2\pi\sqrt{(2)(1)}\cdot(22.51\times10^3)(50\times10^3)} = 100\,pF$$

5) Use equation 5.2

$$f_0 = \frac{1}{2\pi\sqrt{mn}RC} \qquad \rightarrow \qquad R = \frac{1}{2\pi\sqrt{mn}Cf_0}$$

and

$$R = \frac{1}{2\pi\sqrt{mn}Cf_0} = \frac{1}{2\pi\sqrt{(2)(1)}\cdot(100\times10^{-12})(50\times10^3)} = 22.51\,k\Omega$$

As the above procedures showed, choosing the capacitance value in step 2 as the value given from Analog Devices Inc.'s Design Tool gives an identical result for the resistance value in steps 3 and 5. Therefore, using the design procedure from Franco [5] gives the same result as the Analog Devices Inc.'s Design Tool provides.

5.4 PSpice Simulation

The PSpice simulation was ran using the AD8066 circuit file, ad8066.cir, provided from Analog Devices Inc. The simulation schematic is shown in Figure 5-4 and the simulation result is shown in Figure 5-5.

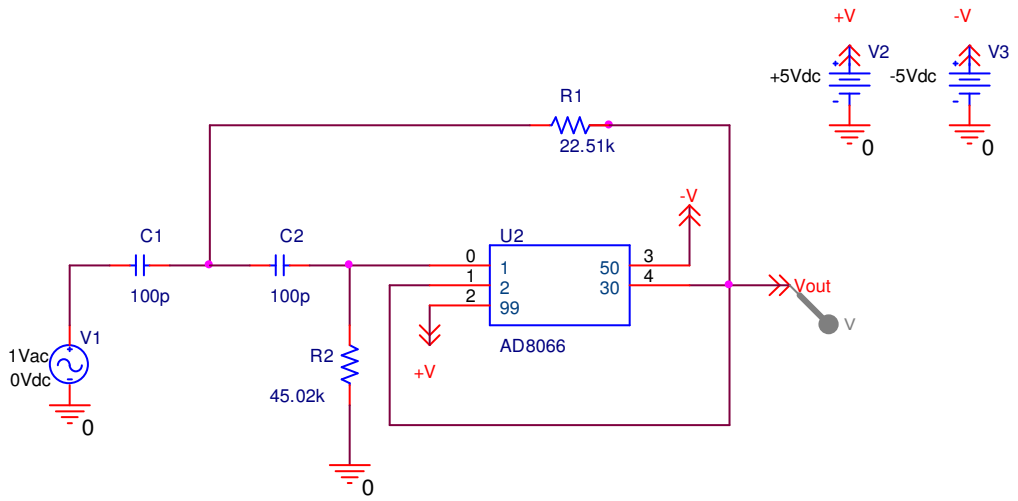

Figure 5-4. PSpice simulation schematic of high pass filter.

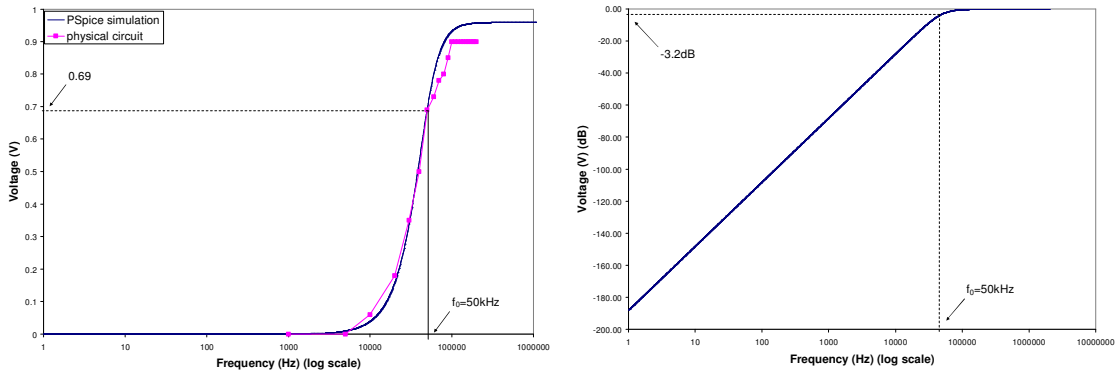

Figure 5-5. PSpice simulation and experimental results of high pass filter shown in Figure 5-4. The figure on the right is in dB scale.

As seen from Figure 5-5, the output voltage at the cutoff frequency, 50 kHz, is about 0.69 V, which is close to the expected value of 0.707. The ideal result is a zero output voltage from DC to the cutoff, then a vertical straight line running up to 1 volt at the cutoff and an output of 1 volt from the cutoff. But this is the ideal "brick wall" case and can never be achieved in real life. If a steeper attenuation is required, high order filter can be used. Also, note that the output pass-band voltage is not quite at 1V, but about 0.95V. Within the margin of errors, this is reasonable. Given the errors from using a breadboard, the component tolerance issue and human error from reading an oscilloscope, the physical circuit response follows the PSpice simulation result quite closely.

6 Development of Low Pass Filter

A low pass filter is basically the opposite of a high pass filter. It is used to attenuate the high frequency content of a signal and allow only the low frequency content of the signal to pass through. Therefore, a low pass filter combined with a high pass filter forms a band-pass filter. The most common low pass filter is the Sallen-Key low pass filter. The Sallen-Key configuration is a second order active filter, which rolls off the unwanted frequency content in the stop-band at 40 dB per decade. High order filters can be built by cascading two or more second order filters together. Typically speaking, the higher the order, the steeper the roll off will be. Figure 6-1 presents the Sallen-Key low pass filter circuit. Note that the only difference a low pass filter has from a high pass filter is that the resistors and capacitors are switched placed.

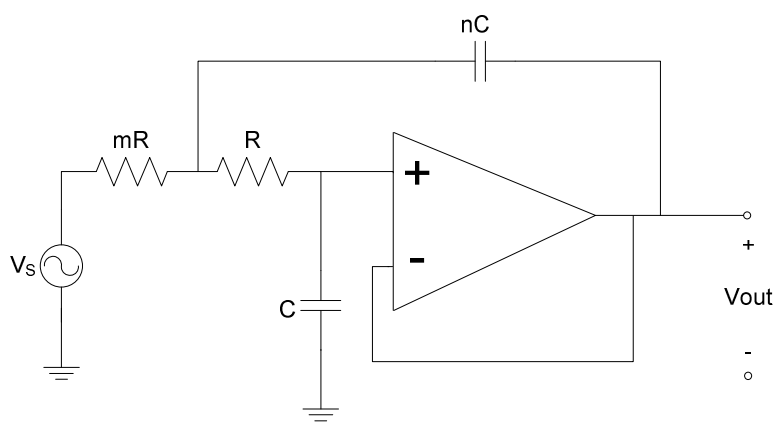

Figure 6-1. Sallen-Key second order low pass filter [5].

The transfer function of the low pass filter is very similar to the transfer function of a high pass filter, the only difference is in the numerator,

$$TF = \frac{1}{1-(f/f_0)^2 + (j/Q)(f/f_0)} \tag{6.1}$$

where the cutoff frequency, f_0 is

$$f_0 = \frac{1}{2\pi\sqrt{mn}RC} \tag{6.2}$$

and the Q value is

$$Q = \frac{\sqrt{mn}}{n+1} \tag{6.3}$$

which are the same equations as equations 5.1 and 5.2. As the same as the high pass filter, the value of Q can range from 0.2 to 100, with values near unity being the most common. A common value for Q is 0.707, which is the lowest Q value before the response starts peaking. Figure 6-2 shows the magnitude plot for a standard low pass filter.

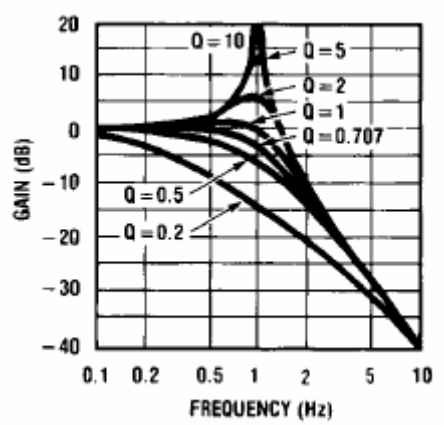

Figure 6-2. Magnitude plot for a typical second order low pass filter [15].

As the same as the high pass filter, the design process of a low pass filter involves choosing the order of the filter, choosing the Q value and picking out the resistors and capacitors suitable for the circuit. The low pass filter in this research was also designed two ways using the Design Tools from Analog Devices Inc. and the step by step design procedure from Franco [4]. Both of these designs, along with the PSpice simulation results and physical circuit results will be presented in the following sections.

6.1 Selection of Op Amps and Design Parameters

This initial design of the low pass filter is a fourth order Butterworth Sallen-Key low pass filter with a cutoff frequency of 1.5 MHz and a Q value of 0.541 for the first stage and a Q value of 1.307 for the second stage. The initial op amp selected was the OP249, which is a Dual JFET high speed op amp. Its applications include instrumentation amplifiers and active filters. However, the OP249 has a gain-bandwidth product of only 4.7 MHz, which we found to be insufficient for our application. Therefore, the final op amp selected for the low pass filter was the same as for the high pass filter, the AD8066. This was a wise choice since the knowledge gained from using the AD8066 for the high pass filter can be applied directly to the low pass filter.

As the same as the high pass filter, the circuit file for the AD8066 was used for the simulation in PSpice. Resulting circuits were built and tested using a breadboard to compare the results to the PSpice simulation results. However, since the PSpice version used was the demo version and is limited to 64 nodes, cascading two op amps together in one simulation program would exceed the maximum number of nodes allowed. Therefore, two different PSpice simulations were performed, one for each stage of the two stage low pass filter.

6.2 Low Pass Filter Design from Analog Devices Inc.

The design from Analog Devices Inc.'s Interactive Design Tools: Op Amps: Active Filter Synthesis has the parameters shown in Figure 6-3. This is a fourth order Butterworth Sallen-Key low pass filter with a cutoff frequency of 1.5 MHz and a *Q* value of 0.541 for the first stage and a *Q* value of 1.307 for the second stage.

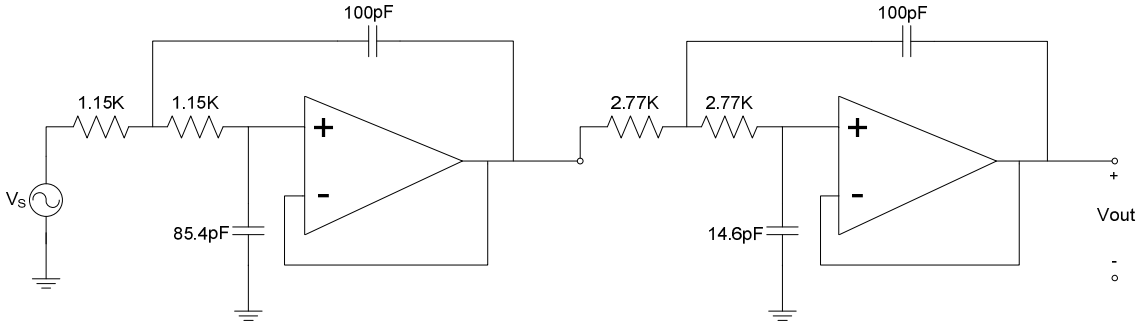

Figure 6-3. Fourth order low pass filter from Analog Device Inc.'s Design Tools with a cutoff frequency of 1.5 MHz and a Q_1 of 0.541 for the first stage and a Q_2 of 1.307 for the second stage [11].

6.3 Low Pass Filter Design Step by Step Procedure

The design procedure offered from Franco [5] has the following procedures to design a low pass filter. This procedure follows the circuit shown in Figure 6-1 and is as follow:

1) Pick two equal resistors (m = 1) in the kΩ range. Call this value R^*.
2) Calculate $C^* = \dfrac{1}{4\pi Q f_0 R^*}$.
3) Calculate $n^* = 4Q^2$.
4) Find the closest capacitors C and nC so that $C \approx C^*$ and $n \geq n^*$.
5) Use the value of n (not n^*) found in 4) to compute the quantity $k = \dfrac{n}{Q^2} - 2$. Then compute $m = \dfrac{k + \sqrt{k^2 - 4}}{2}$.
6) Use equation 6.2, $f_0 = \dfrac{1}{2\pi\sqrt{mn}RC} \rightarrow R = \dfrac{1}{2\pi\sqrt{mn}f_0 C}$ to compute R.
7) Select standard resistors closest to R and mR.

Using the above procedures with a cutoff frequency of 1.5 MHz and a Q_1 = 0.541 for the first stage:

1) Choose R^* = 1.15 kΩ and m = 1. (The same R value as given from Analog Devices Inc.'s Design Tool).

2) $C^* = \dfrac{1}{4\pi Q f_0 R^*} = \dfrac{1}{4\pi(0.541)(1.5\times10^6)(1.15\times10^3)} = 85.3pF$.

3) $n^* = 4Q^2 = 4(0.541)^2 = 1.17$.

4) Suppose C = C^* = 85.3 pF and n = n^* = 1.17, then nC = 100 pF.

5) $k = \frac{n}{Q^2} - 2 = \frac{1.17}{0.541^2} - 2 = 2$

$$m = \frac{k + \sqrt{k^2 - 4}}{2} = \frac{2 + \sqrt{2^2 - 4}}{2} = 1.$$

6) $R = \frac{1}{2\pi\sqrt{mn}\, f_0 C} = \frac{1}{2\pi\sqrt{(1)(1.17)}(1.5\times10^6)(85.3\times10^{-12})} = 1.15k\Omega.$

7) This can be accomplished from combing resistors in series and parallel configurations to get the proper resistance values.

Using the same procedures with a cutoff frequency of 1.5 MHz and a Q_2 = 1.307 for the second stage:

1) Choose R^* = 2.8 kΩ and m = 1. (The same R value as given from Analog Devices Inc.'s Design Tool).

2) $C^* = \frac{1}{4\pi Q f_0 R^*} = \frac{1}{4\pi(1.307)(1.5\times10^6)(2.8\times10^3)} = 14.5pF$.

3) $n^* = 4Q^2 = 4(1.307)^2 = 6.83$.

4) Suppose $C = C^*$ = 14.5 pF and $n = n^*$ = 6.83, then nC = 100 pF.

5) $k = \frac{n}{Q^2} - 2 = \frac{6.83}{1.307^2} - 2 = 2$

$$m = \frac{k + \sqrt{k^2 - 4}}{2} = \frac{2 + \sqrt{2^2 - 4}}{2} = 1$$

6) $R = \dfrac{1}{2\pi\sqrt{mn}\,f_0 C} = \dfrac{1}{2\pi\sqrt{(1)(6.83)}\,(1.5\times10^{6})(14.5\times10^{-12})} = 2.8k\Omega$

7) This can be accomplished from combing resistors in series and parallel configurations to get the proper resistance values.

As the above procedures showed, choosing the resistance value in step 1 as the value given from Analog Devices Inc.'s Design Tool would result in an identical result for the capacitance value in steps 2 and 4 for both the first and second stages. This proofs that both designs are the same.

6.4 PSpice Simulation

The PSpice simulation was ran using the circuit file for AD8066 provided in the Analog Devices Inc.'s website. As mentioned before, due to the 64 node limitation of the demo version PSpice, the first stage and second stage of the low pass filter cannot be put together in one simulation. A different simulation had to be run for each stage. Figures 6-4 and 6-5 present the PSpice schematic, simulation results and physical circuit results for the first stage; Figures 6-6 and 6-7 present the PSpice schematic, simulation results and physical circuit results for the second stage.

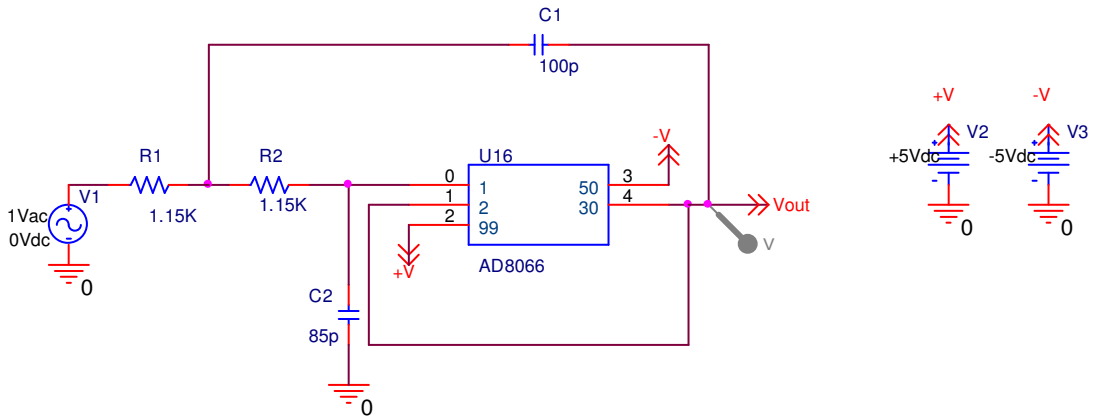

Figure 6-4. PSpice simulation schematic for first stage of low pass filter.

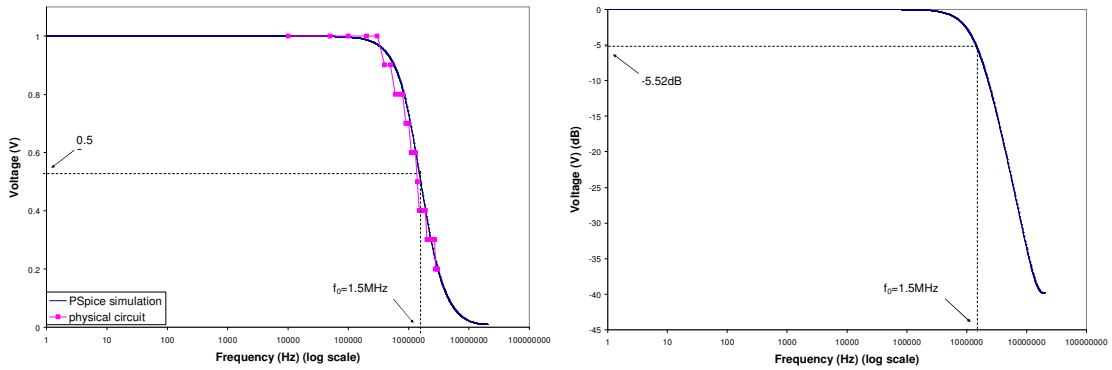

Figure 6-5. PSpice simulation and physical circuit results for first stage of low pass filter. The figure on the right is in dB scale.

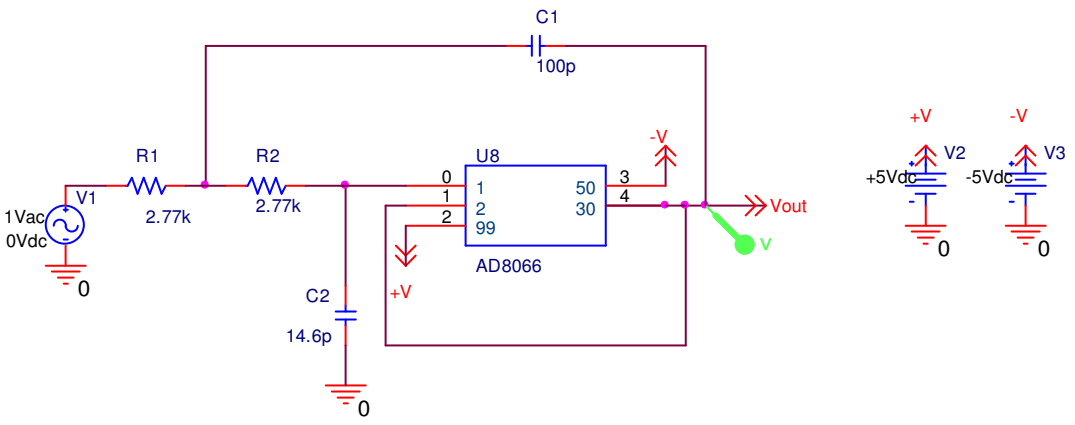

Figure 6-6. PSpice simulation schematic for second stage of low pass filter.

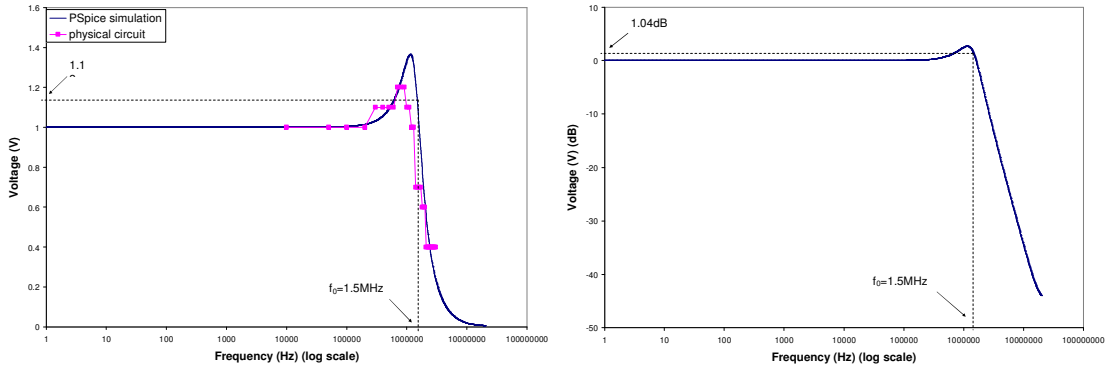

Figure 6-7. PSpice simulation and physical circuit results for second stage of low pass filter. The figure on the right is in dB scale.

The advantage of a high order filter can be seen from Figures 6-5 and 6-7. Note that the output voltage of the first stage (Figure 6-5) starts to roll off before the cutoff frequency of 1.5 MHz. However, the output voltage of the second stage (Figure 6-7) peaks up and then rolls off. Therefore, when combining the two voltages together, the peaking from the second stage would actually cancel out the early roll off from the first stage. The end result is a steeper roll-off. This can be seen in Figure 6-8.

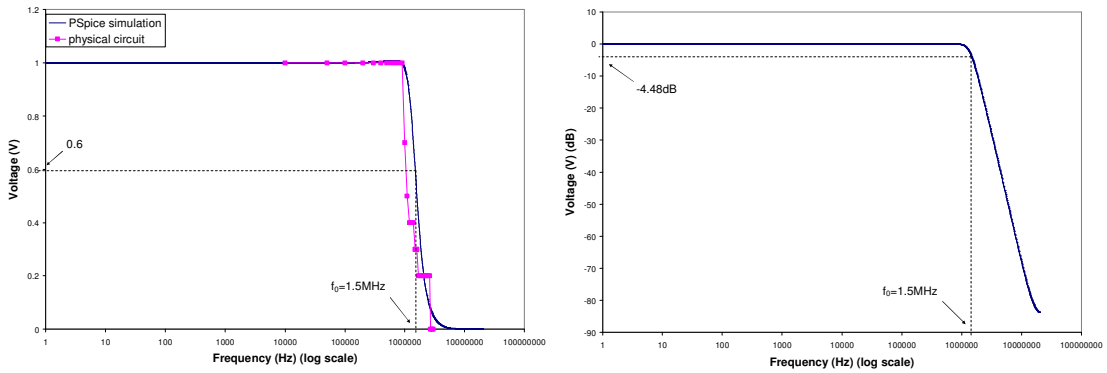

Figure 6-8. PSpice simulation and physical circuit results for combining the first and second stage results of low pass filter. The figure on the right is in dB scale.

Figure 6-8 shows that at the cutoff frequency of 1.5 MHz, the voltage is approximately 0.6. Under ideal situation, the response should be 0.707 at the cutoff frequency. The percent error of 0.6 is

$$Percent\ \ Error = \frac{|0.6 - 0.707|}{0.707} \times 100 = 15\%$$

This percent error is due to the op amp imperfection and the modeling of the actual op amp using PSpice.

7 Development of Line Driver

The purpose of a line driver is to increase the current of the input signal from a function generator into the piezoelectric sensors. A line driver is necessary because the input current from a function generator is not high enough to drive the piezoelectric sensors, which require a current of a few hundred mA to actuate. A line driver is a simple op amp circuit and thus does not have any specific configurations like the charge amplifier and the high pass and low pass filters. As long as the op amp used for the line driver has a high enough output current, the circuit configuration is not important. For this application, the line driver can simply be configured as a voltage follower with gain.

The research effort for designing the line driver was focused on 1) testing several different op amps to see if the output current of each op amp is high enough; and 2) testing a special feature that some of these op amps have: the Power Down feature. The Power Down feature is basically a digital logic gate that possesses a threshold voltage from one of the pins on the op amp chip. If the applied voltage to this logic gate is above the threshold voltage, the op amp will let the incoming signal pass through to its output. If this logic gate is below the threshold voltage, the op amp will block the incoming signal so that the output will be close to zero. This feature can be though of as an on and off switch of the op amp. When the switch is on, the op amp lets the input signal pass through. When the switch is off, the op amp blocks the input signal from passing through. Figure 7-1 shows the difference in output of an op amp for the two power-down settings.

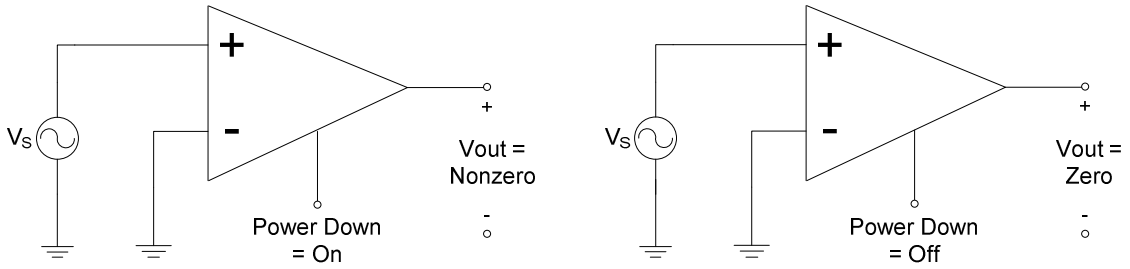

Figure 7-1. Power down is on, output is nonzero (left). Power down is off, output is zero (right).

7.1 Selection of Op Amp and Design Parameters

As mentioned in the previous section, the research effort on the line driver was focused on studying and testing several op amps to see if a suitable one can be found. The op amps studied were the AD8390, AD8392 and AD8019.

7.1.1 AD8390

The AD8390 is a low power, high output current differential amplifier whose applications include DSL line driver and high current differential amplifier. The AD8390 has an output current of 400 mA when driving a 10 Ω resistance load. This output current is enough for our application since the maximum output current desired was 300 mA. The AD8390 uses two pins to control the power down option. These two pins are PWDN0 and PWDN1 with a digital reference ground pin called DGND. The purpose of the power down pins is for power management. When the op amp is not being used, it can be set to the down level so that the internal biased current, or quiescent supply current, I_Q, can be lowered to save power consumption. I_Q is the current that keeps the internal transistors of the op amp properly biased during operation. When this current is set to be close to zero, the op amp will be idle.

Both PWDN0 and PWDN1 pins can be set to a value of 1 or 0, therefore, there are a total of four levels. These four levels correspond to four different quiescent supply current levels. From the data sheet, the quiescent supply current corresponding to each power level is as follow:

(PWDN1, PWDN0) = (1,1) => I_Q = 10.0 mA
(PWDN1, PWDN0) = (1,0) => I_Q = 6.7 mA
(PWDN1, PWDN0) = (0,1) => I_Q = 3.8 mA
(PWDN1, PWDN0) = (0,0) => I_Q = 0.67 mA

Therefore, if the op amp is desired to be at operation, one should set the (PWDN1, PWDN0) to (1,1); if the op amp is desired to be idle, one should set it to (0,0). The two intermediate levels are for fine tuning.

There is also a current adjustment pin, I_{ADJ}, that would allow the quiescent current to be further fine tuned. The I_{ADJ} is also a 1 or 0 digital logic gate, and thus with the addition of this pin, there can be a total of eight levels for the quiescent current. However, this IADJ was not necessary for the op amp to operate and thus was not tested.

The main reason these power down pins are advantageous for this application is that when the piezoelectric sensors are operating in the actuating direction, the line driver can operate in the (1,1) mode and thus allow the output signal from the function generator to pass through. When the sensors are operating in the sensing direction, the line driver can operate in the (0,0) mode and thus block the output signal from the function generator. However, from testing, it was found that these power down pins did not perform as well as the data sheet stated. When the (PWDN1, PWDN0) pins were set to (0,0), a noticeable amount of current was still observed at the output of the op amp. This led to an exploration of a different op amp.

7.1.2 AD8392

After testing the power down pins on the AD8390 and finding out it was not working as well as it intended, we moved on to the AD8392. The AD8392 is a low power, high output current line driver, with four identical op amps inside the chip. It has an output current of 400 mA driving a 10 Ω resistor. There are two sets of power down pins, with each set controlling two op amps. These power down pins function just like the power down pins on the AD8390. However, this AD8392 was not actually tested because we believed that it is an identical op amp as the AD8390, except that the AD8392 consists of four individual identical op amps, while the AD8390 has only one. Therefore, the AD8392 would function the same as the AD8390, except one AD8392 is equivalent to four AD8390. Because we believed that the power down pins on the AD8390 did not work properly, then the AD8392 would perform the same as the AD8390 and thus no further testing was done on the AD8392.

7.1.3 AD8019

After studying both AD8390 and AD8392 and finding that the power down options didn't work as well as the data sheets stated, we moved on to another op amp, the AD8019. The AD8019 is a DSL line driver also with a power-down feature. The AD8019 has an output current of 200 mA driving a 25 Ω load. While this may not be enough for our application, this op amp was a good stopping point in terms of feasibility of the power down feature. We believed that if the power-down feature still does not work for this op amp, then it may be wise to move on to different vendors for this particular application. The AD8019 has one PWDN pin and one DGND pin. The basic function of these pins are the same as the ones on the AD8390 and the AD8392. The PWDN is a digital logic gate and can take the value of 1 or 0, depending on the voltage applied to it. If a voltage above the threshold voltage is applied to the PWDN pin, then a value of 1 is read and the op amp is on. If a voltage below the threshold voltage is applied to it, then a value of 0 is read and the op amp is off. This threshold voltage is 1.8 V. The DGND pin is the digital reference ground pin.

The data sheet stated that if the PWDN is supplied with a 5 V, then the supply current is 9 mA; if the PWDN is supplied with a 0 V, then the supply current is 0.8 mA. We tested the supply currents at both the positive and negative supply pins and the output current at both power on and power off options. While there was a significant decrease in current readings when the PWDN was connected to ground, however, these current readings were not as low as what the data sheet stated. The main concern was the output current. In the ideal situation, we want the output current to be whatever value it should be when PWDN = 5 V, and to be zero when PWDN = 0 V. However, the output current tested was never close to zero.

The other problem with the AD8019 was the supply voltage. The AD8019 was rated to operate at a maximum of ±12 V. However, it was found that as soon as the supply voltage was set above 5 V, the chip started to get hot. If the supply voltage was

set close to 12 V, smoke started to come out of the chip and eventually the chip would burn. This was also very disturbing.

After studying three different possible line driver op amps from Analog Devices Inc. and found out that they did not perform the way they should, the engineers at Triad Semiconductors Inc. decided to move on to a different vendor. Three other op amps were chosen. These are the LM8272 and LM7372 from National Semiconductors and OPA633 from Texas Instruments. Because of scheduling issue, no testing was performed on these op amps in this research work.

8 Conclusion and Future Work

The work of this thesis focused on supporting the ongoing project to build a well packaged, prototype structural health monitoring system using off-the-shelf electronics. Funding of this project came from the Air Force. Triad Semiconductors was appointed to build the electronics and data acquisition system. The University of South Carolina provides the expertise in active lamb wave. The North Carolina A&T State University provides the expertise in passive acoustic emission. The work on this thesis focuses on learning the two different techniques and testing various operational amplifiers used in the system. All of the testing work done described in this thesis was to support the design of the system.

8.1 Conclusion from Research Work

This structural health monitoring system consists of many components such as the analog electronics, piezoelectric sensors and data acquisition system. Out of these, the four major components used in the analog electronics are charge amplifier, high pass filter, low pass filter and line driver. Testing of different op amps for feasibility to be used for these four components, as well as designing the circuits were the core of this research work. The purpose of a charge amplifier is to bring down the high impedance signal from a piezoelectric sensor to a low impedance signal. It was found that there are two possible circuits to perform this task and op amp AD745 was chosen for this application.

A high pass filter is to attenuate the low frequency content of a signal and allow only the higher frequency content to pass through. A low pass filter is the opposite of a high pass filter. A low pass filter is to attenuate the high frequency content of a signal and allow only the lower frequency content to pass through. The op amp chosen for this application was the AD8066 and the design of these two filters came from Analog Devices Inc.'s website "Interactive Design Tools: Op Amps: Active Filter Synthesis".

A line driver is to drive the low current signal from a function generator to a higher current signal for actuation of the piezoelectric sensors. Several op amps were tested for this application, but a satisfactory op amp has not been found. At this point, no op amp has been finalized for this application yet.

PSpice was used for all the computer simulations for the various circuits. The main reason PSpice was used is because Analog Devices Inc. provides PSpice circuit files for the majority of their products. The newer version of PSpice also offers a user friendly schematic input interface, which makes it very easy to use. The ability to simulate the result of a circuit before actually building it saved a tremendous amount of time in the design process. When a possible design exists, a prototype circuit can be built, tested, and compared with the simulation result. It was found that for all of the circuits tested, the physical circuit results resemble quite closely to the simulation results from PSpice, given the errors involved from reading an oscilloscope and using a breadboard. Appendix B presents some pictures of the instruments used for building and testing circuits.

This thesis concluded that using off-the-shelf electronic components to build a prototype health structural monitoring system is feasible. Different commercial op amps were tested and found that they are suitable for this application. While there are still many issues to be solved, a working prototype is not far from being finished.

8.2 Future Work

Of the four major components discussed in this thesis, the charge amplifier, high pass filter and low pass filter designs have been finalized for this project. The op amp selection of the line driver is still a question at this point. The line driver requires an op amp with a high enough output current. PCB circuit boards have been made and tested. A switch matrix was also added to the circuitry to allow the system to work on different piezoelectric sensors.

A data acquisition system needs to be implemented for sending input signals to the piezoelectric sensor and receiving output signals from the sensors. This data acquisition system should be implemented using LabView, since LabView provides a user friendly interface and is widely used in the industry. It is believed that engineers at Triad Semiconductors Inc. may have completed this task.

Once the system is finalized and tested, a total of three systems need to be built. One system will go to The University of South Carolina for the active lamb wave testing; one system will go to The North Carolina A&T State University for the passive acoustic emission testing; and one system will go to the Air Force for real aircraft panel testing. The ultimate task will involve combining the active lamb wave technology and the passive acoustic emission technology together to test real aircraft panels provided by the Air Force. This is the initial goal that this project was intended to accomplish.

8.3 Final Remark

After working on this project, I have found that my knowledge in the electrical engineering field to be very limited. At the beginning of the design and testing phase of the project, I found myself spending lots of time trying to understand the data sheet. The lack of soldering skill was also a major drawback. Working with breadboard has been a frustrating, but rewarding experience once the circuit finally worked. The lack of an understanding of the underlying issues such as added stray capacitances working with breadboard was probably one of the biggest hurdles I encountered. The fact that I did not know a PCB board would provide a much better and consistent result than breadboard was a constant struggle as I was always trying to get the "perfect" result, which is close to being impossible on breadboard. This is just one of the many issues that I dealt with. While my skills and understanding have improved over time during this project, it is far from being mature.

I strongly feel that this experience has made me realize the undergraduate mechanical engineering program at Virginia Tech lacks hands-on electronic experience. While students are required to take both Electrical Theory and Industrial Electronics, it is still far from being enough. Courses such as Digital Signal Processing, Mechatronics and Instrumentations need to be incorporated into the undergraduate curriculum to give students a better understanding of hands-on electronics . While mechanical engineers in the industry still work on traditional mechanical engineering disciplines such as machine design and thermal analysis, more and more engineers are becoming multi-disciplined. With the direction in which technology is heading, a good understand of basic electronics is not only important, but crucial.

Appendix A

Steps to get a schematic model from a vendor circuit file for a specific op amp.

1) In Windows Explorer, make a copy of the circuit file and change the extension of one of the two circuit file from "cir" to ".lib".
2) Start the PSpice Model Editor (not Capture).
3) Choose File, Create Capture Parts.
4) In the box that says 'Enter Input Model Library", browse to find the file modified in step 1.
5) Click OK to start.
6) A message log will appear, and if the circuit file downloaded has no errors, it should show 0 errors.
7) Two files are created. The first file has extension "lib" and is the error log file. The second file has extension "LIB" and is the actual model that can be placed into PSpice.
8) To place the new part in a schematic: in Capture, choose Place Parts. Click "Add Library" and browse to the second file created in step 7 with extension "LIB", then open.
9) A new part will show up under Part List and the model can now be placed onto a schematic.
10) For these models, the parts placed on the schematic don't necessarily look like the universal symbols that most people are familiar with. For example, an op amp will appear as a box with the inverting and non-inverting inputs, the positive and negative power supplies and the output instead of the familiar triangle shape. In order to distinguish the pins, open the original circuit file downloaded and the pins are assigned at the line that says ".SUBCKT".
11) In order for the model to work correctly, in the simulation setting, click the tab "Libraries." Under filename, browse to the circuit file "cir" downloaded. Click Add as Global or Add to Design. Add as Global allows the model to be used on all PSpice files, while Add to Design only allows the application at hand to use the model.

Appendix B

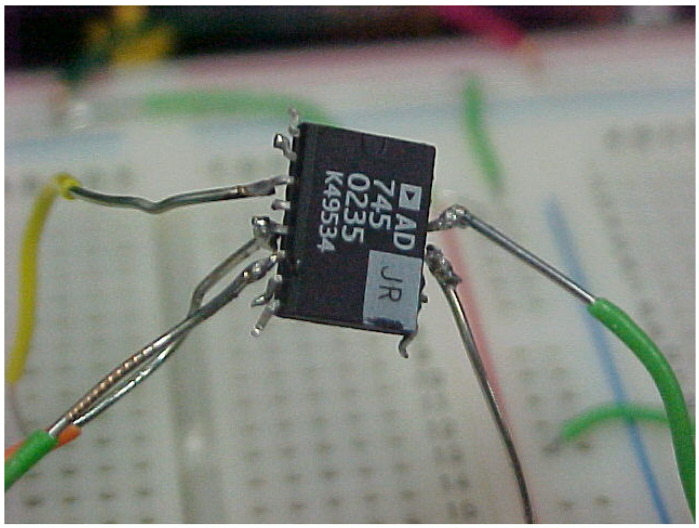

Figure B-1. Wires soldered on surface mount (SOIC) op amp for use on breadboard before the use of SOIC to DIP adapters.

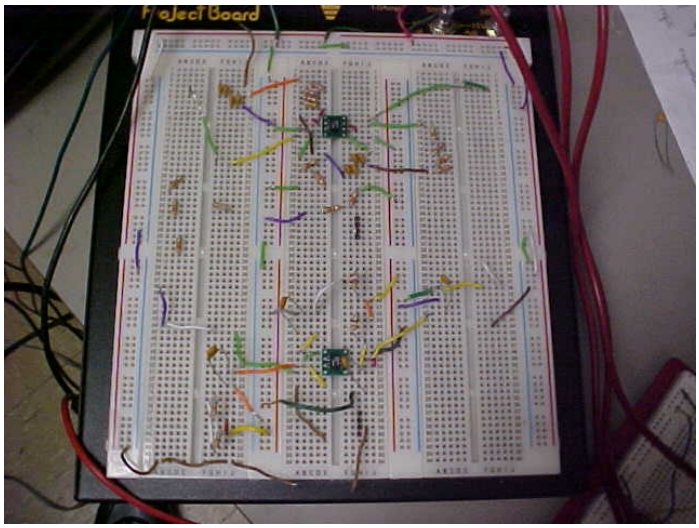

Figure B-2. Design and testing of high and low pass filters.

Figure B-3. Instruments used for testing include function generator, multimeter and oscilloscope.

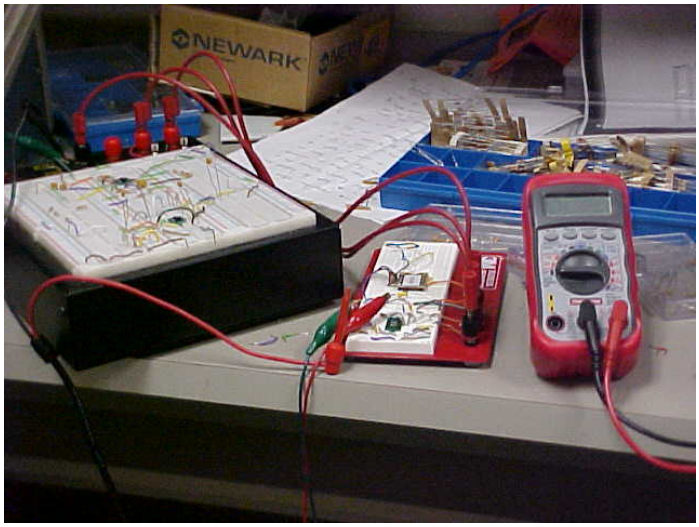

Figure B-4. Testing of line driver involves measuring the current with a multimeter.

References

[1] Beattie, A. G., "Acoustic Emission, Principles and Instrumentation," *Journal of Acoustic Emission*, vol. 2, no. ½ (1983), pp. 95-128.

[2] Datta, S., Kirikera, G. R., Schulz, M. J., and Sundaresan, M. J., "Continuous Sensors for Structural Health Monitoring," *Proceedings of SPIE*, vol. 5046 (2003), pp. 164-175.

[3] "Elastic Waves – A Demonstration, Laboratory For Active Materials And Smart Structures, Center for Mechanics of Materials and Non-Destructive Evaluation, Mechanical Engineering, University of South Carolina" http://www.me.sc.edu/Research/cmmnde/ (June 2000)

[4] Finlayson, R. D., Friesel, M. A., Carlos, M. F., Miller, R., Godinez, V., "Acoustic Emission Structural Health Management Systems (AE-SHMS)," *Proceedings of SPIE*, vol. 3994 (2000), pp. 128-137.

[5] Franco, S., *Design with Operational Amplifiers and Analog Integrated Circuits* (New York: McGraw-Hill Companies, Inc., 1988).

[6] Giurgiutiu, V., "Active Sensors for Health Monitoring of Aging Aerospace Structures," *Preceedings of SPIE*, vol. 3985 (2000), pp. 294-305.

[7] Giurgiutiu, V., Bao, J., and Zhao, W., "Active Sensor Wave Propagation Health Monitoring of Beam and Plate Structures," *Proceedings of SPIE*, vol. 4327 (2001), pp.234-245.

[8] Giurgiutiu, V. and Lyshevski, S. E., *Micromechatronics Modeling, Analysis, and Design with MATLAB* (Boca Raton, Florida: CRC Press LLC, 2004)

[9] Giurgiutiu, V., Bao, J., and Zhao, W., "Piezoelectric Wafer Active Sensor Embedded Ultrasonics in Beams and Plates," *Society for Experimental Mechanics*, vol. 43 (2003), pp.428-449.

[10] Giurgiutiu, V., "Lamb Wave Generation with Piezoelectric Wafer Active Sensors for Structural Health Monitoring," *Proceedings of SPIE*, vol. 5056 (2003), pp. 111-122.

[11] "Interactive Design Tools: Op Amps: Active Filter Synthesis," http://www.analog.com/Analog_Root/static/techSupport/designTools/interactiveTools/filter/filter.html.

[12] Kehlenbach, M., and Das, S., "Identifying Damages in Plates by Analyzing Lamb Wave Propagation Characteristics," *Proceedings of SPIE*, vol. 4702 (2002), pp. 364-375.

[13] Kester, W., Wurcer, S., and Kitchin, C., *Section 5 High Impedance Sensors*, Analog Devices, Inc.

[14] Kirikera, G., Datta, S., Schulz, M. J., Ghoshal, A., Sundaresan, M. J., Feaster, J., and Hughes, D., "Recent Advances in an Artificial Neural System for Structural Health Monitoring," *Proceedings of SPI*E, vol. 5046 (2003), pp. 152-163.

[15] Lacanette, K., *A Basic Introduction to Filters – Active, Passive, and Switch-Capacitor*, National Semiconductor, application note 779 (April 1991).

[16] Leo, D., "ME 5984 Smart Structures/Active Materials," ME 5984 course note, Virginia Tech, 2003.

[17] Martin, W. N., Ghoshal, A., Sundaresan, M. J., Lebby, G. L., Schulz, M. J., and Pratap, P. R., "Artificial Nerve System for Structural Monitoring," *Proceedings of SPIE*, vol. 4702 (2002), pp. 49-62.

[18] Pfleiderer, K., Stoessel, R., and Busse, G., "Health Monitoring Techniques Using Integrated Sensors," *Proceedings of SPIE*, vol. 5046 (2003), pp.224-231

[19] Raj, B., and Jha, B. B., "Principles & Techniques Fundamentals of Acoustic Emission," *British Journal of NDT*, vol. 36, no. 1 (January 1994), pp. 16-23.

[20] Rizzoni, G., *Principles and Applications of Electrical Engineering*, 4th ed. (New York: McGraw-Hill Companies, Inc., 2004).

[21] Sirohi, J., and Chopra, I., "Fundamental Understanding of Piezoelectric Strain Sensors," *SPIE Conference on Smart Structures and Integrated Systems*, vol. 3668 (March 1999), pp. 528-542.

[22] Tront, J. G., *PSpice For Basic Circuit Analysis* (New York: McGraw-Hill Companies, Inc., 2004)

[23] "Tyco Electronics," http://www.amp.com/products/technology/articles/interface.stm (July 1995).

.

Vita

Yiu Kui Law was born in Hong Kong on March 16, 1980. He moved to the United States at the age of 15 on August 1995. He has ever since lived in the state of Virginia. In 1998, he graduated from Oakton High School and decided to attend Virginia Tech to study mechanical engineering. He received his Bachelor of Science in Mechanical Engineering from Virginia Tech in May 2003, graduating Magna Cum Laude.

During his undergraduate career at Virginia Tech, he was a member of several honor societies such as Pi Tau Sigma, Tau Beta Bi and Golden Key. He also participated in the co-operative program working at the General Motors Baltimore Truck Assembly Plant in Baltimore, MD and Dupont Lycra® Research and Development in Waynesboro, VA.

In May 2003, he entered graduate school at Virginia Tech to pursue his Master of Science degree in Mechanical Engineering. He started this research project with Dr. Wicks in September 2004. Upon completion of this degree, he will work for the Westinghouse Electric Company in Monroeville, PA.